





Article

African Vulture Optimization Algorithm-Based PI Controllers for Performance Enhancement of Hybrid Renewable-Energy Systems

Ghazi A. Ghazi ^{1,2,*} , Hany M. Hasanien ³ , Essam A. Al-Ammar ^{1,2} , Rania A. Turkey ⁴, Wonsuk Ko ¹ , Sisam Park ⁵ and Hyeong-Jin Choi ⁵

- ¹ Electrical Engineering Department, Faculty of Engineering, King Saud University, Riyadh 11421, Saudi Arabia; essam@ksu.edu.sa (E.A.A.-A.); wkoh@ksu.edu.sa (W.K.)
 - ² K. A. CARE Energy Research and Innovation Center, King Saud University, Riyadh 11421, Saudi Arabia
 - ³ Electrical Power and Machines Department, Faculty of Engineering, Ain Shams University, Cairo 11566, Egypt; hanyhasanien@ieee.org
 - ⁴ Electrical Engineering Department, Faculty of Engineering and Technology, Future University in Egypt, Cairo 11835, Egypt; rania.turky@fue.edu.eg
 - ⁵ GS E&C Institute, GS E&C Corp., 33, Jong-ro, Jongno-gu, Seoul 03159, Korea; parkss7@gsenc.com (S.P.); hjchoi@gsenc.com (H.-J.C.)
- * Correspondence: 439106681@student.ksu.edu.sa; Tel.: +966-538634823

Abstract: An effective maximum power point tracking (MPPT) technique plays a crucial role in improving the efficiency and performance of grid-connected renewable energy sources (RESs). This paper uses the African Vulture Optimization Algorithm (AVOA), a metaheuristic technique inspired by nature, to tune the proportional–integral (PI)-based MPPT controllers for hybrid RESs of solar photovoltaic (PV) and wind systems, as well as the PI controllers in a storage system that are used to smooth the output fluctuations of those RESs in a hybrid system. The performance of the AVOA is compared with that of the widely used the particle swarm optimization (PSO) technique, which is commonly acknowledged as the foundation of swarm intelligence. As a result, this technique is introduced in this study to draw a comparison. It is observed that the proposed algorithm outperformed the PSO algorithm in terms of the tracking speed, robustness, and best convergence to the minimum value. A MATLAB/Simulink model was built, and optimization and simulation for the proposed system were carried out to verify the introduced algorithms. In conclusion, the optimization and simulation results showed that the AVOA is a promising method for solving a variety of engineering problems.

Keywords: maximum power point tracking; PI controllers; hybrid system; African Vulture Optimization Algorithm (AVOA); renewable-energy sources



Citation: Ghazi, G.A.; Hasanien, H.M.; Al-Ammar, E.A.; Turkey, R.A.; Ko, W.; Park, S.; Choi, H.-J. African Vulture Optimization Algorithm-Based PI Controllers for Performance Enhancement of Hybrid Renewable-Energy Systems. *Sustainability* **2022**, *14*, 8172. <https://doi.org/10.3390/su14138172>

Academic Editor: Manosh C. Paul

Received: 31 May 2022

Accepted: 29 June 2022

Published: 4 July 2022

Publisher's Note: MDPI stays neutral with regard to jurisdictional claims in published maps and institutional affiliations.



Copyright: © 2022 by the authors. Licensee MDPI, Basel, Switzerland. This article is an open access article distributed under the terms and conditions of the Creative Commons Attribution (CC BY) license (<https://creativecommons.org/licenses/by/4.0/>).

1. Introduction

The world today is confronted with a slew of challenging energy issues, which have become worse in recent years because of rapidly expanding energy demands. Global energy demand is expected to rise by 44% between 2006 and 2030, according to the International Energy Agency [1]. Traditionally, fossil-fuel reserves have not been a viable alternative for future usage, as they are unable to meet the world's expanding needs and contribute to environmental pollution, global warming, climate change, and ozone-layer destruction. As a result, clean energy generated by renewable-energy sources (RESs) is becoming increasingly significant in the generation of power.

Due to these key aspects, RESs appear to be a viable choice for green energy production. RESs are indeed clean, safe, and sustainable. Solar and wind energy, among the various types of RESs, have become the most essential because they are the most widely used and dispersed around the world and can meet all of humanity's needs [2]. A microgrid is a self-sufficient energy micro-system that can run in both a parallel mode with distribution

systems and an island mode. Furthermore, it can be connected to various power-generation systems including RESs. A microgrid has proven to improve power quality, reduce power losses, and reduce emissions [3]. Moreover, a microgrid's islanding capability during faults or disturbances in power-system networks would improve grid and customer reliability. In [4], a PV-fed DC microgrid is described for a fault detection and localization, while analyzing different faults such as line-to-line and line-to-ground in different parts of the microgrid.

Solar energy is generated when sunlight is converted to electricity using semiconductor materials. In the PV system, the maximum power point (MPP) of a solar cell's non-linear power voltage (P-V) characteristic is unique, and it fluctuates in response to the ambient temperature and solar irradiation. As a result, an MPP tracker is necessary to ensure that the MPP remains operational regardless of the weather conditions. In the previous two decades, a significant amount of the literature has been documenting the various types of MPPT algorithms utilized in optimizing the energy of PV arrays, including traditional techniques such as perturb and observe [5], hill-climbing [6] and incremental conductance [7], fractional open-circuit voltage [8], and fractional short-circuit current [9]. However, due to partial shading, these may just be stuck in one of the local maxima and fail to track the MPP. The MPP has been tracked using intelligent methods such as the fuzzy logic controller [7], artificial neural network [10], and genetic algorithm [11]. These methods, however, need substantial training and experience in a challenging setting.

Recently, considerable research has revealed a strong desire in bioinspired MPPTs, which have outperformed intelligent methods such as the PSO [12], artificial-bee colony [13], grey-wolf-optimization technique [14], firefly algorithm [15], salp-swarm optimization [16], ant-colony optimization [17], and cuckoo-search algorithm [18] in various environmental conditions. Moreover, several research works have incorporated these methods into hybrid ones to improve their performance and eliminate their drawbacks, specifically, by integrating the optimization ability of various searching mechanisms into an incorporated form of at least two methods, to recover the limitations of one method via the performance of another [19].

Moreover, in the literature, several algorithms for tracking the maximum power in wind systems have been presented, including using a radial-basis function via the neural network control strategy [20], grasshopper-optimization algorithm [21], power-capture optimization [22], perturb-and-observe-based higher-order sliding-mode controller [23], Archimedes optimization algorithm [24], mechanical-senseless method [25], neuro-adaptive generalized global sliding-mode controller [26], artificial intelligence-based adaptive perturb-and-observe controller [27], and MPPT based on integrated generator-rectifier systems [28].

Depending on the operating status of the PV or wind systems, the MPPT approaches generate reference signal (positive or negative). The predicted reference signal identifies the systems' trajectory. Most of these approaches are reliable and accurate in a steady state, but they suffer when the load or environmental conditions varies quickly. Due to solar radiation and wind speed having an intermittent nature, the output power of PV and wind systems fluctuates. Before sending power to the grid, those power fluctuations must be smoothed down. As a result, a variety of strategies have been used to smooth the output power of RESs systems, such as using storage devices. The integration of energy-storage devices into RESs has a significant impact on the output-power-smoothing issue. In general, battery-storage devices are effectively used to smooth the output power of RESs [29].

Generally, a power electronic-converter interface between the source and load is incorporated in wind and solar systems. This converter setup allows these systems to use the maximum power available, regardless of the environmental conditions. The error between the output PV/wind system's voltage and the MPPT algorithm's reference voltage is used to control the converter's electronic switches, which are minimized by using lots of controllers such as slide-mode control [30], fuzzy logic [31], feedback linearization [32], a proportional-integral-derivative (PID) controller [33], conventional proportional plus

integral (PI) [34], etc. Nonetheless, using certain controllers in the industry is limited due to practice and sophisticated computations. Therefore, due to the PI controllers' resilience and wide-range stability margins, these controllers are still the most widely employed in the industry. These controllers, however, are sensitive to adjustments in elements and system nonlinearities. As a result, optimal tuning of these controllers is the best-suited approach for regulating the hybrid system with grid-connected renewable-power generation.

Several optimization algorithms were proposed for tuning the PI controllers in many engineering applications, such as the genetic algorithm [35], grey-wolf optimizer [36], whale-optimization algorithm [37] and intelligent-based fuzzy methods such as the fuzzy logic controller [38], fuzzy-genetic controller [39], swarm-optimization- and pattern-search-based fuzzy controller [40], and differential-evolution-based fuzzy controller [41], which are applied to tune the PI controllers gain used in several power applications. Moreover, metaheuristic techniques such as the cuckoo-search algorithm [42], PSO [43], and bees algorithm [44] are viable options for fine-tuning the settings of PI controllers. One of the recently developed metaheuristic algorithms is the AVOA. This algorithm has been applied to solve various engineering problems such as optimization of parameter identification for solid-oxide fuel cells [45] and proton exchange membrane (PEM) fuel-cell stacks [46], and the optimal design of a hybrid RES [47]. It has more inclusive exploration and exploitation mechanisms. The usage of a random approach enhances the exploration and exploitation abilities of both mechanisms. This approach can ensure that the AVOA will not only skip a local optimum and have quick convergence but also guarantee that it is not too divergent [48].

In this paper, the incremental-conductance method is applied, which is one of the maximum power point tracking algorithms that is extensively used because it has high tracking correctness and high productivity in rapidly changing atmospheric conditions. This algorithm, combined with PI controllers, is used to obtain the MPPT in PV and wind systems. In addition, the AVOA is proposed for tuning the gains of the PI controllers of the converters' electronic switches, the Generation Side Converters (GSCs), in the PV, wind, and storage systems of the whole hybrid system. The GSC is properly regulated by the incremental-conductance-based PI controller, to efficiently control the MPP of the PV and wind systems. In addition, tuning the PI controllers in the storage system produces the firing pulses of the GSC for optimal charge and discharge, to smooth fluctuations in the output of renewable systems, because of the irregular nature of wind speed and solar irradiance. The tuning of PI controllers using the AVOA is compared with the PSO method. The PSO method is a bio-inspired technique that takes advantage of the communal intelligence of identical individuals to maximize the efficiency of the search operation. This technique is regarded as the foundation of swarm intelligence [49]. Thus, this technique is presented to gain a comparison in this paper. The key contributions of this paper are listed in the following points:

- Applying the incremental-conductance method combined with the PI controllers for the MPP tracking of PV and wind systems.
- Introducing a novel algorithm called the African Vultures Optimization Algorithm for tuning the PI controllers in the hybrid system.
- Comparing the results of the application of the AVOA with the PSO method.
- Implementing a storage system to smooth the fluctuations in the output of renewable systems, i.e., wind and PV systems, because of the irregular nature of wind speed and solar irradiance.

The structure of the article is as follows: The components of hybrid RESs in detail are pointed out in Section 2. The methodology, which includes the incremental conductance and African Vulture Optimization Algorithms, is provided in Section 3. Section 4 presents and discusses the optimization and simulation results. Finally, in Section 5, the conclusions of the study are introduced.

2. Hybrid DC Microgrid System

The hybrid system involves AC, PV, wind, and storage systems connected with different DC loads, of 10 kW, 30 kW, 40 kW, and 50 kW, was proposed. The parameters of the hybrid system are illustrated in Appendix A (Tables A1–A6). In this system, the incremental conductance method combined with the PI controllers for tracking the MPP of PV and wind systems was implemented. In addition, the AVOA was introduced for tuning the PI controllers that were proposed in the system.

2.1. AC System

In this study, the AC system of 100 kW consists of three voltage source, a transformer, and a universal bridge that works as voltage-source converter (VSC), which is connected to the DC microgrid as depicted in Figure 1. The VSC controller consists of voltage and current regulators that are connected to a pulse-width modulation (PWM) controller that is responsible for producing the firing pulses to the VSC.

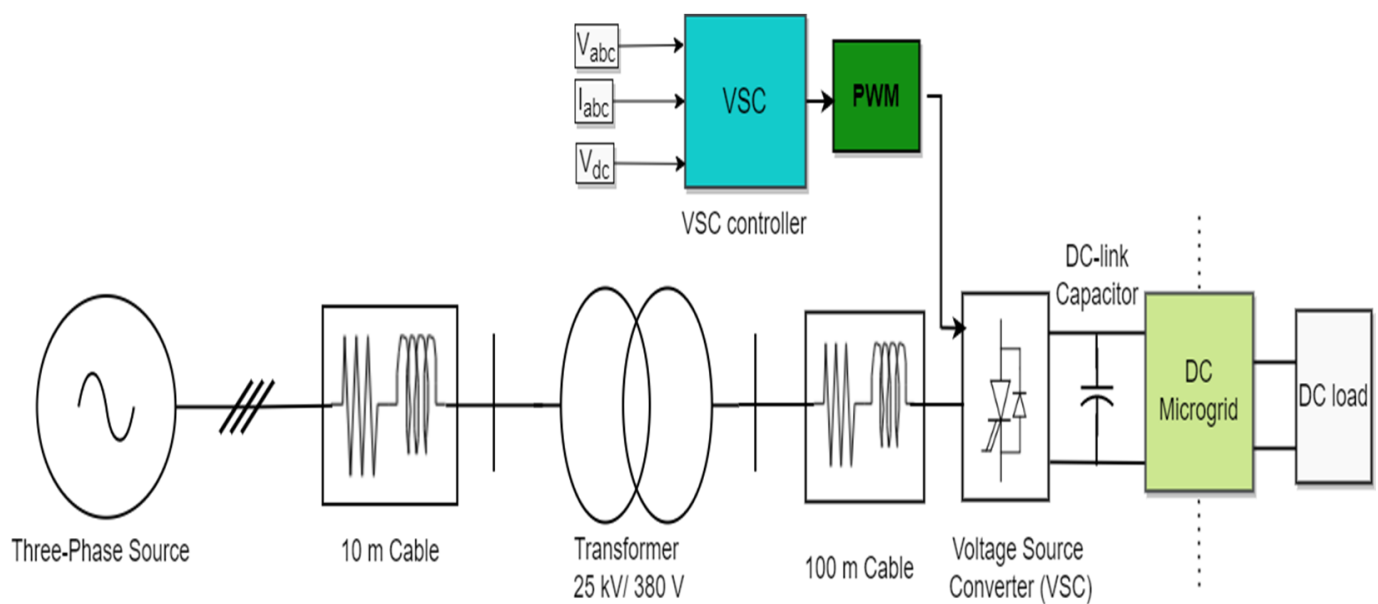


Figure 1. The on-grid AC system with voltage-source converter.

2.2. PV System

The proposed layout of a 20 kW on-grid PV system is shown in Figure 2. A PV array with many PV modules connected in parallel and in a series makes up this system. The terminal of the PV array is linked to a boost converter, which regulates the array's terminal voltage and transmits the maximum power to a DC link connected to a DC microgrid with DC loads. Figure 3 depicts a one-diode model of the PV cell. Equation (1) is used to calculate the PV cell's output current [50]. The output voltage and current of the PV array can be calculated according to the number of modules in a series and in parallel in the array. Irradiance (shown in Figure 4) and temperature curves (shown in Figure 5) are the PV array's inputs, which were taken from a weather-monitoring station at King Saud University, Riyadh, Saudi Arabia. In addition, Figure 6 shows the PV array's P–V characteristic curve.

The output current of a PV cell can be calculated using Equation (1) as follows:

$$I = I_L - I_0 \left[\exp \left(\frac{q(V_D + IR_S)}{\eta kT} \right) - 1 \right] - \frac{V + IR_S}{R_{SH}} \quad (1)$$

Here, I_L denotes the photocurrent, I_0 represents the reverse saturation current, V_D is the diode's voltage, η is the semiconductor constant, q is the magnitude of the electric

charge, T represents the absolute temperature in kelvin, k is Boltzmann's constant, and V is the PV cell's output voltage.

2.3. Wind System

In this system, a variable-speed, variable-pitch wind turbine is under investigation, which is paired with a two-mass drive train that drives a three-phase wound-rotor synchronous generator, as shown in Figure 7. The wind system is proposed to supply the loads with 10 kW. The energy produced by the generator is converted to DC energy, using a rectifier device. The incremental conductance-based PI-controller approach uses the rectifier's terminal voltage and current as inputs to regulate the boost converter's terminal voltage and deliver the maximum power to the DC link, which is connected to a DC microgrid with DC loads. The wind speed [51] was obtained from the state of Arizona, USA, since it has a similar climate as Saudi Arabia, which was taken as an input to the wind system that is displayed in Figure 8.

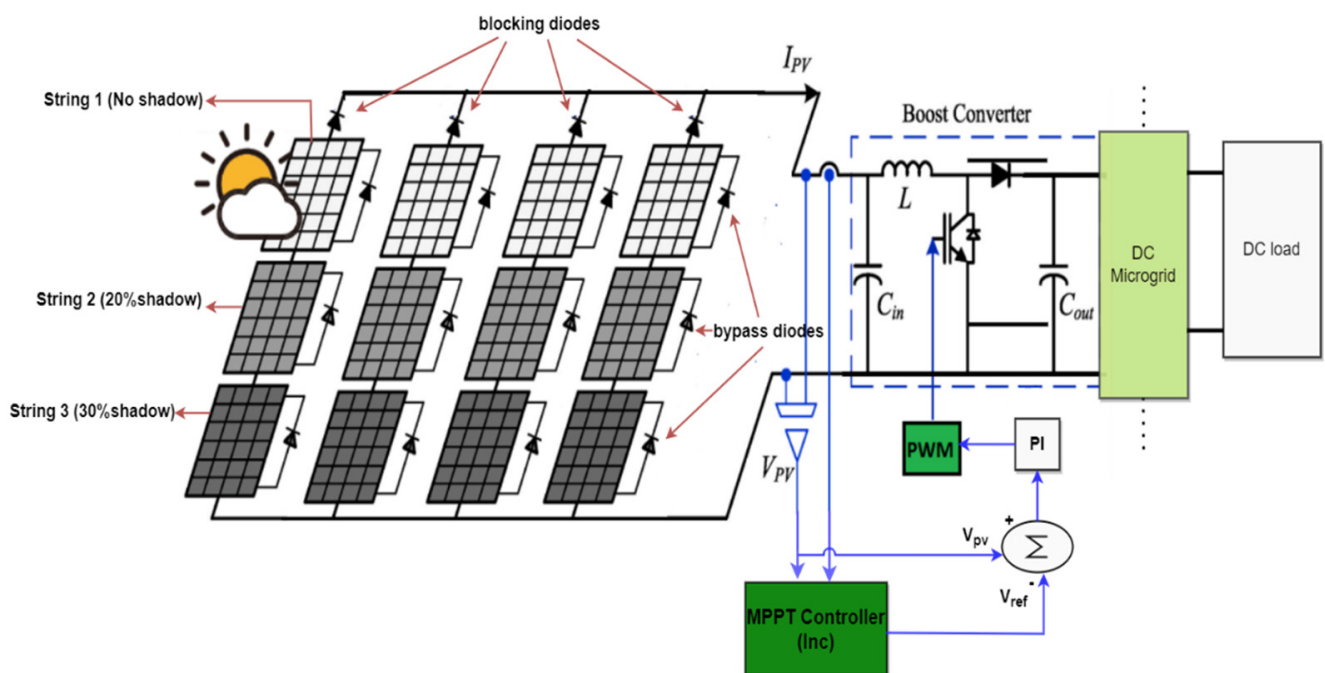


Figure 2. The layout of PV system with an MPPT controller.

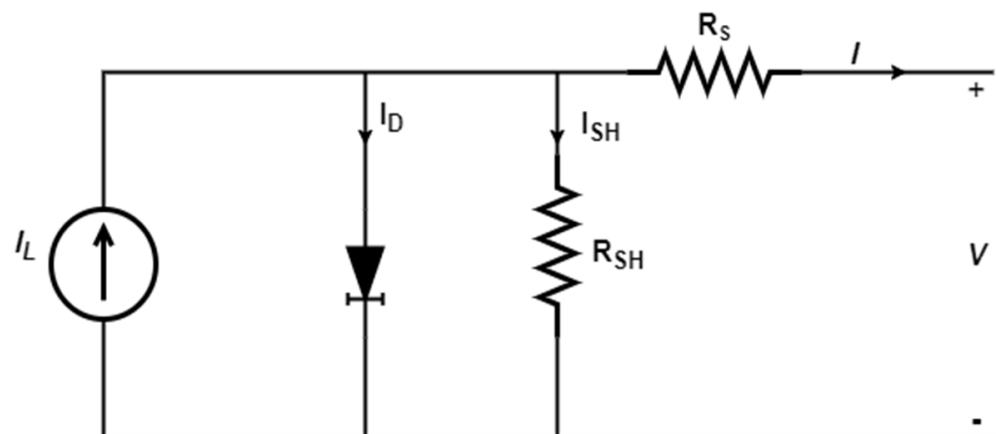


Figure 3. The one-diode PV cell's equivalent circuit.

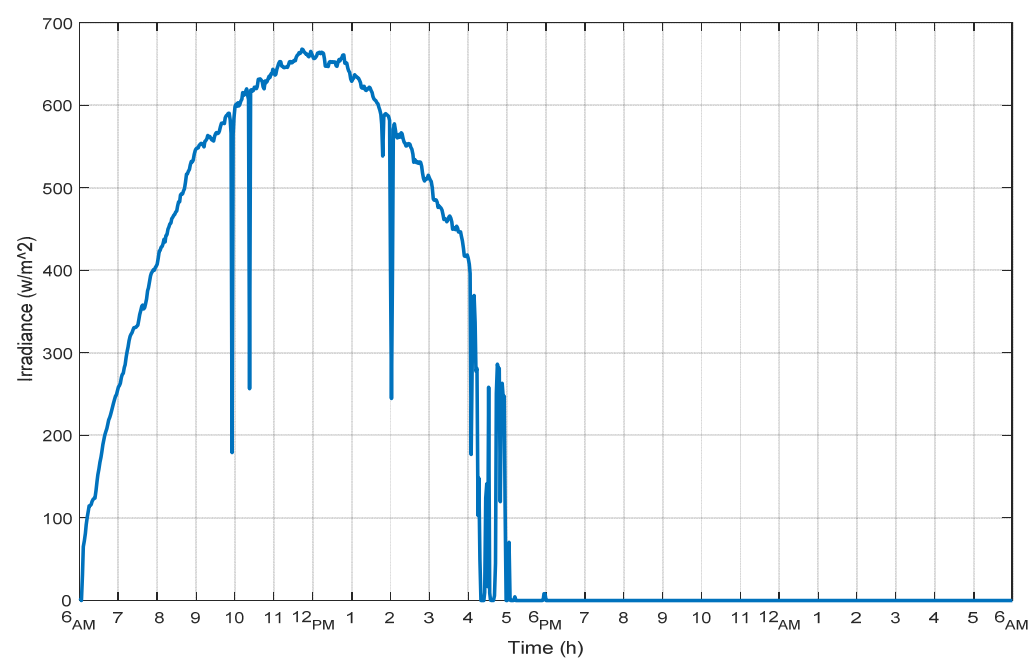


Figure 4. Irradiance.

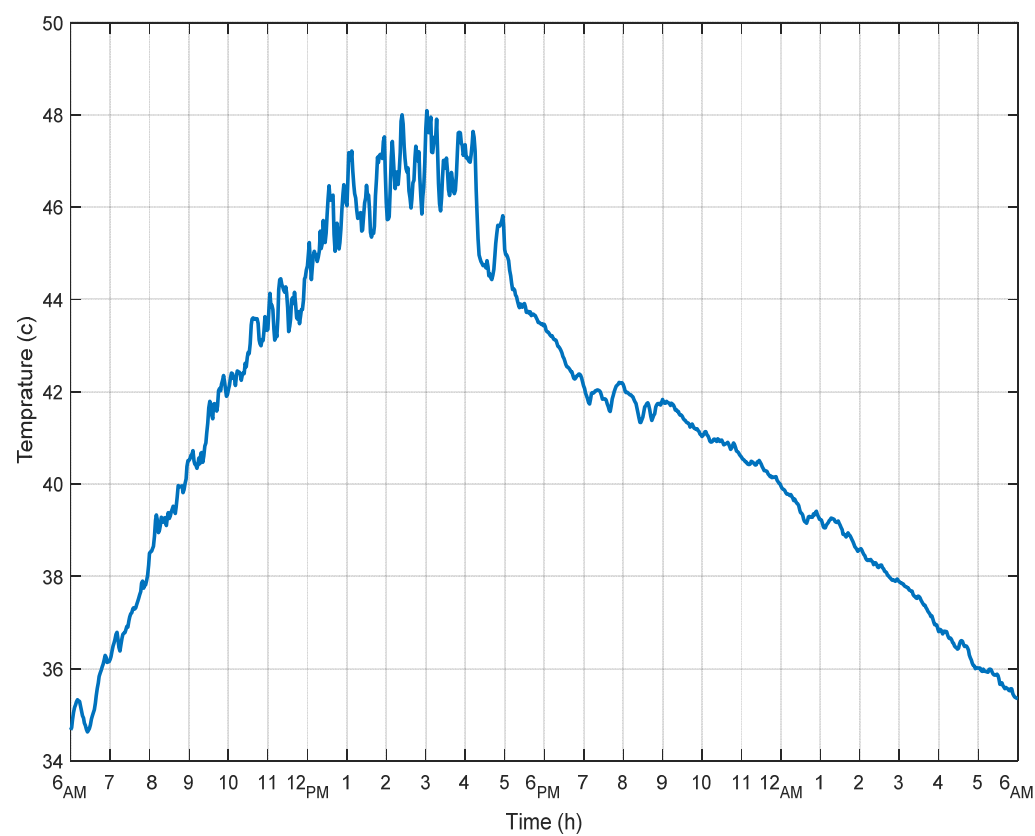


Figure 5. Temperature.

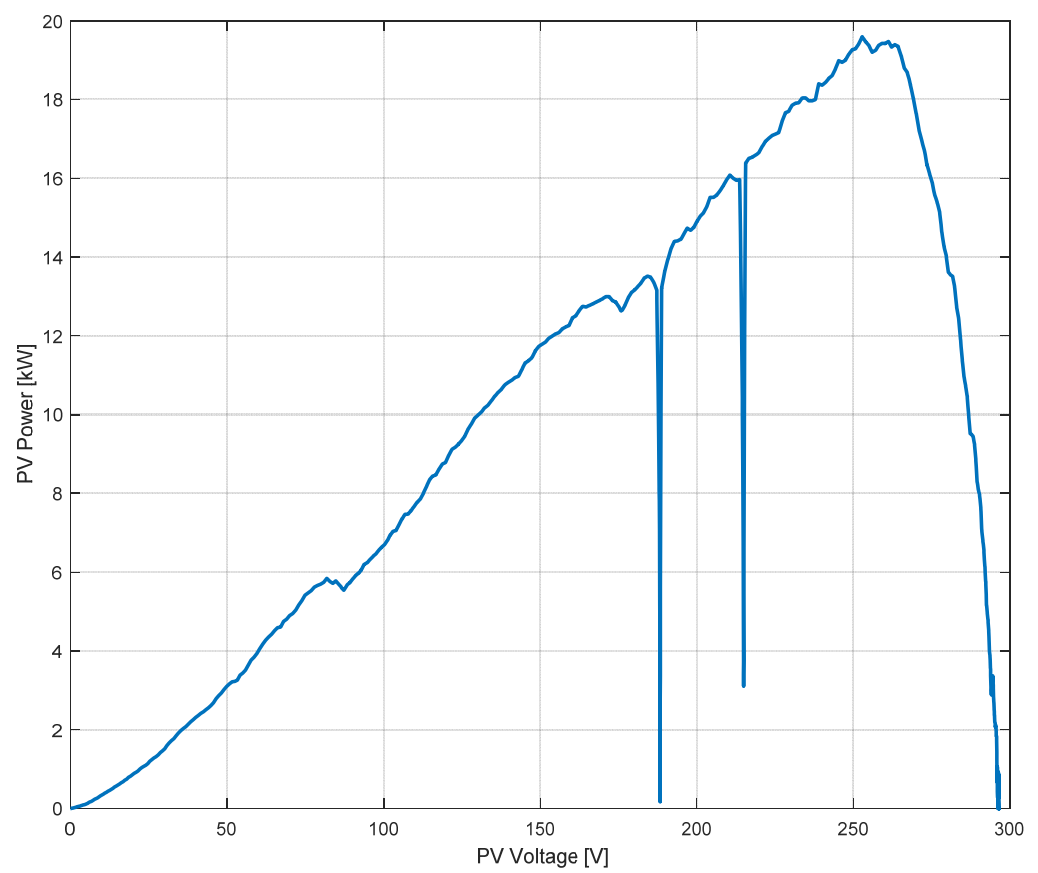


Figure 6. P–V characteristic curve of the PV system.

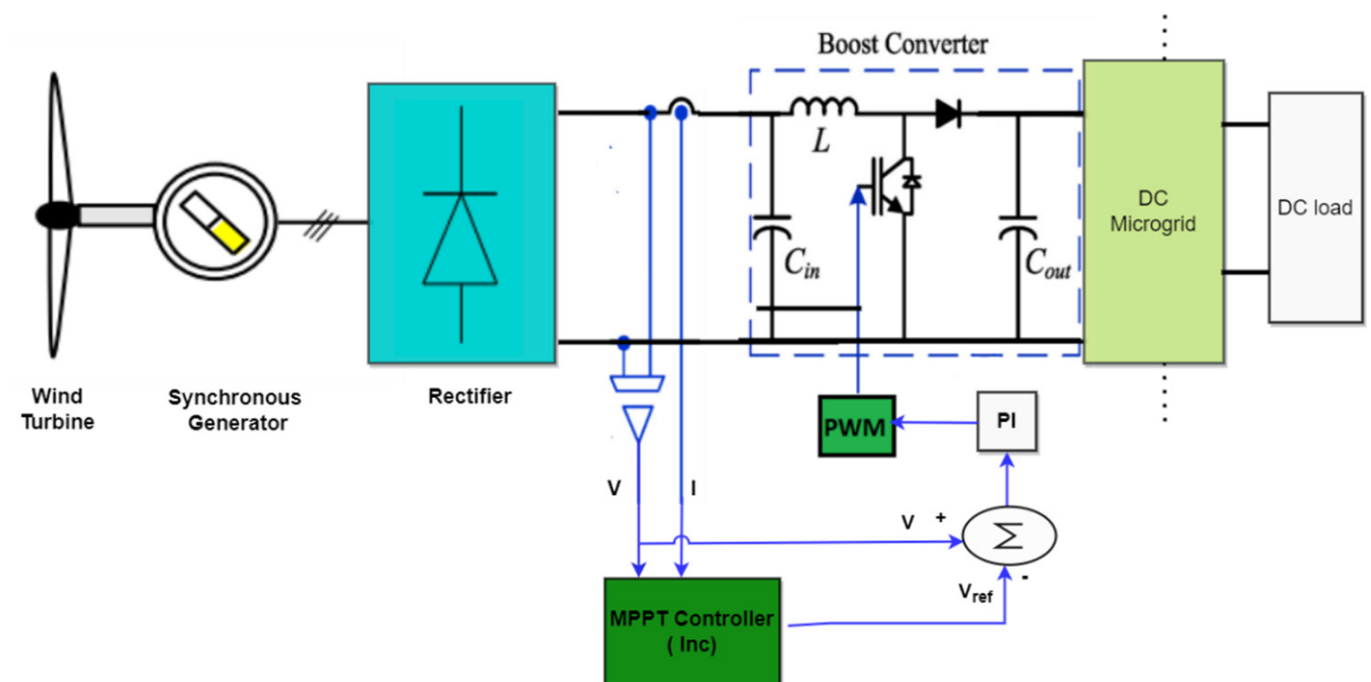


Figure 7. The layout of wind system with an MPPT controller.

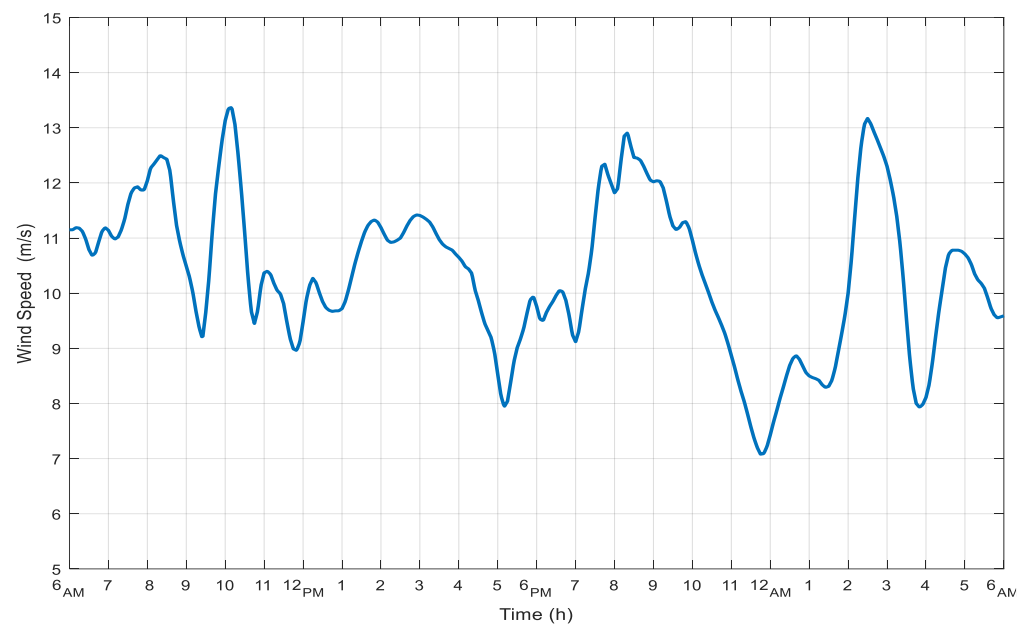


Figure 8. Wind speed.

2.4. Storage System

The on-grid storage system with a capacity of 800 Ah with a nominal 120 V and 50% state of charge (SOC) is connected to a DC microgrid in the hybrid system to smooth fluctuations in the output of PV and wind systems because of the irregular nature of the wind speed and solar irradiance, as shown in Figure 9. In the storage system, a bi-directional buck-boost converter is used to either charge the battery or discharge its energy to the system, according to the energy fluctuations of the PV and wind systems.

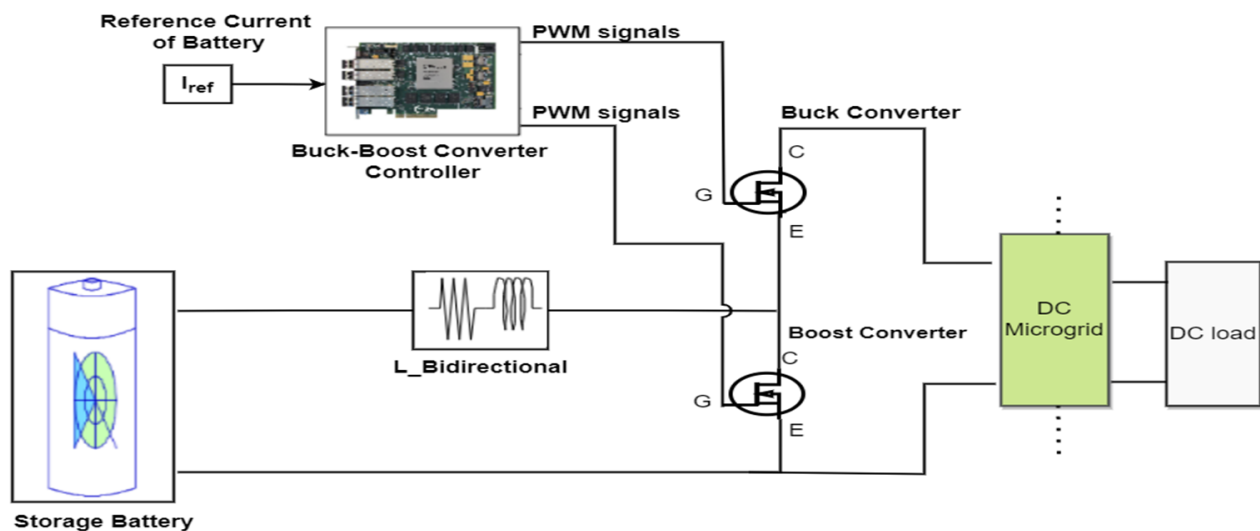


Figure 9. The on-grid storage system.

3. Methodology

To track the maximum power of solar and wind systems, the incremental conductance algorithm is used. Furthermore, the African Vulture Optimization Algorithm is utilized to identify the optimal values of PI-controller gains in PV, wind, and storage systems, and the results are compared to the PSO method. The MPPT-objective function can be expressed using Equation (2).

$$\text{Max } P = V \times I \quad (2)$$

Here, I denotes the output current drawn from a PV cell or a wind system's output rectifier, and V is the corresponding output voltage. The integral of time multiplied absolute error (ITAE) criteria, which is provided by Equation (3) [52], was employed as an objective function for PI controller's optimization.

$$\text{Min ITAE} = \int_0^t t |e(t)| dt \quad (3)$$

where, $e(t)$ is the error, which is the difference between the PV/wind system's output voltage and the MPPT method's corresponding reference voltage, or the difference between the battery's output current and the reference charging/discharging current.

3.1. Incremental-Conductance Algorithm

The incremental conductance algorithm was designed using a P–V characteristic curve observation. This algorithm was developed in 1993 to address some of the shortcomings of the perturb-and-observe technique [53]. Under rapidly changing weather conditions, the incremental-conductance algorithm tries to improve tracking time and yield more energy. The slope of the P–V characteristic curve of the PV array at the *MPP* in this algorithm is zero [54]. As a result, $\frac{\Delta P}{\Delta V} = 0$ with $P = VI$. Similarly, the same principle of this algorithm is applied to the wind system. Consequently, the logic behind the rate of change of current in proportion to the corresponding change in voltage is as follows:

$$\begin{aligned} \frac{\Delta I}{\Delta V} &= -\frac{I}{V} \text{ if } P = \text{MPP} \\ \frac{\Delta I}{\Delta V} &> -\frac{I}{V} \text{ if } P < \text{MPP} \\ \frac{\Delta I}{\Delta V} &< -\frac{I}{V} \text{ if } P > \text{MPP} \end{aligned} \quad (4)$$

and the equation of the incremental conductance method is expressed using Equation (5), as follows:

$$\frac{\Delta P}{\Delta V} = \frac{\Delta(VI)}{\Delta V} = I \frac{\Delta V}{\Delta V} + V \frac{\Delta I}{\Delta V} = I + V \frac{\Delta I}{\Delta V} \quad (5)$$

In the incremental-conductance algorithm, the *MPP* can be tracked by comparing the instantaneous conductance ($\frac{I}{V}$) with the incremental conductance ($\frac{\Delta I}{\Delta V}$). This algorithm decreases or increases the reference value until it achieves the condition $\frac{\Delta I}{\Delta V} = -\frac{I}{V}$. This method is repeated until the *MPP* is achieved, after which the PV's operation point is re-established at the *MPP*. Figure 10 shows the incremental conductance algorithm's flowchart and processes for calculating the PV array's *MPP*.

3.2. African Vulture Optimization Algorithm

The AVOA, a new nature-inspired metaheuristic algorithm, was introduced by B. Abdollahzadeh, et al. [55]. Figure 11 depicts the flowchart and stages for the proposed AVOA. This algorithm was designed by modeling and simulating the living habits and foraging behavior of African vultures using the following criteria:

1. The African vulture population has N vultures, and each vulture's position space is specified in d dimensions.
2. The population of vultures is separated into three groups. The vultures' quality position is determined by the feasible solution's fitness value; the best solution is recognized as the best and first vulture, the second solution is recognized as the second-best vulture, and the other vultures are assigned to the third group.
3. In the population, the three groups are created so that the most important natural role of vultures could be formulated. As a result, various vulture species play distinct roles.
4. Also, the fitness value of the possible solution can reflect the benefits and drawbacks of vultures. Therefore, the weakest and most hungry vultures correlate to the worst vultures. The strongest and most numerous vultures, on the other hand, correlate to the best vulture at the time. Generally, all vultures in the AVOA aim to be near the best vultures while avoiding the worst.

In the foraging stage, the AVOA method can be separated into five stages based on the above-mentioned four criteria to simulate the behavior of different vultures.

a. Phase 1: Population Grouping

In this phase, following the formation of the initial population, the fitness of all solutions is determined, and the best solution is recognized as the best and first vulture, the second solution is also recognized as the second-best vulture using Equation (6), and the other vultures are assigned to the third group, according to the second criteria.

$$R(i) = \begin{cases} \text{BestVulture}_1 & \text{if } p_i = L_1 \\ \text{BestVulture}_2 & \text{if } p_i = L_2 \end{cases} \quad (6)$$

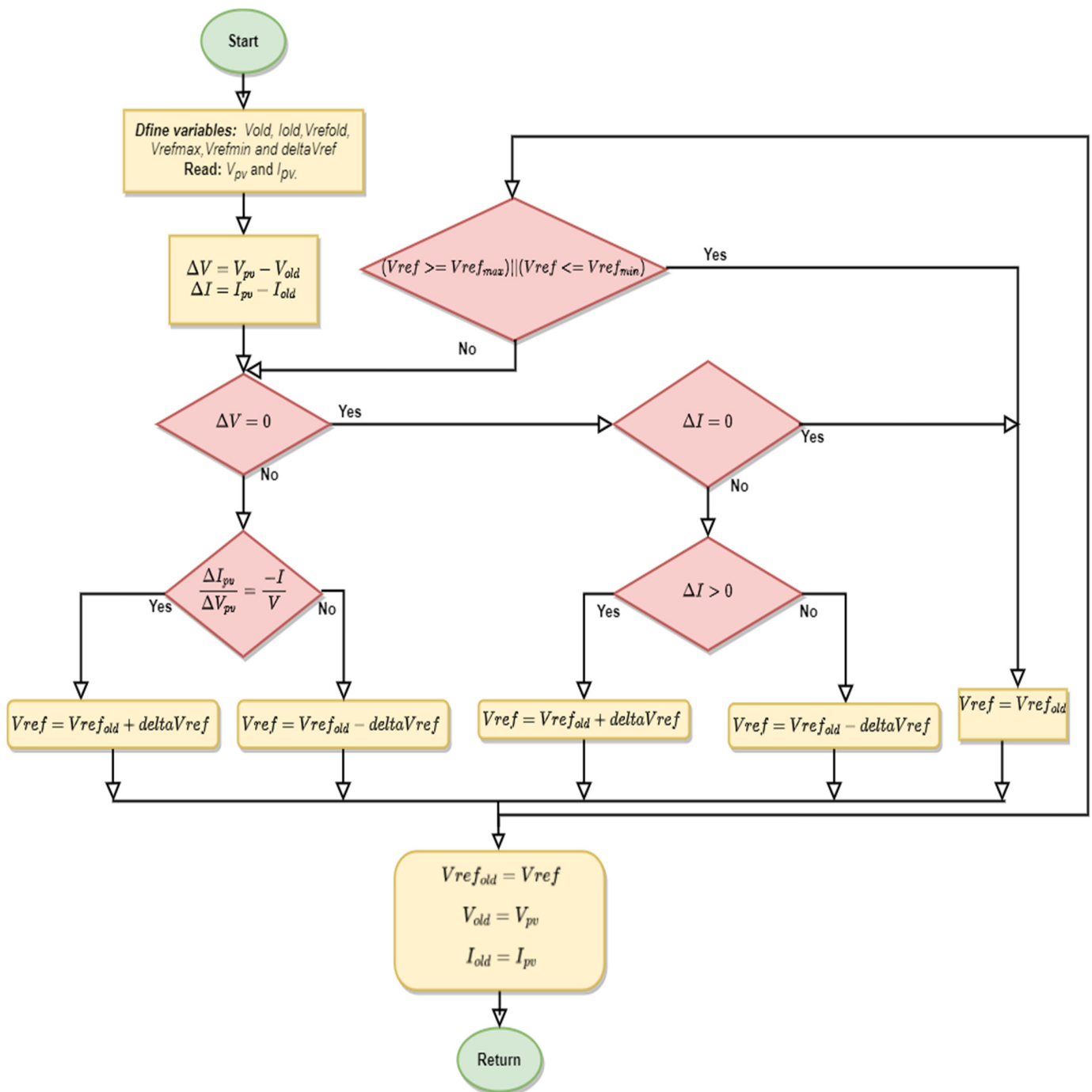


Figure 10. Flowchart of incremental conductance algorithm.

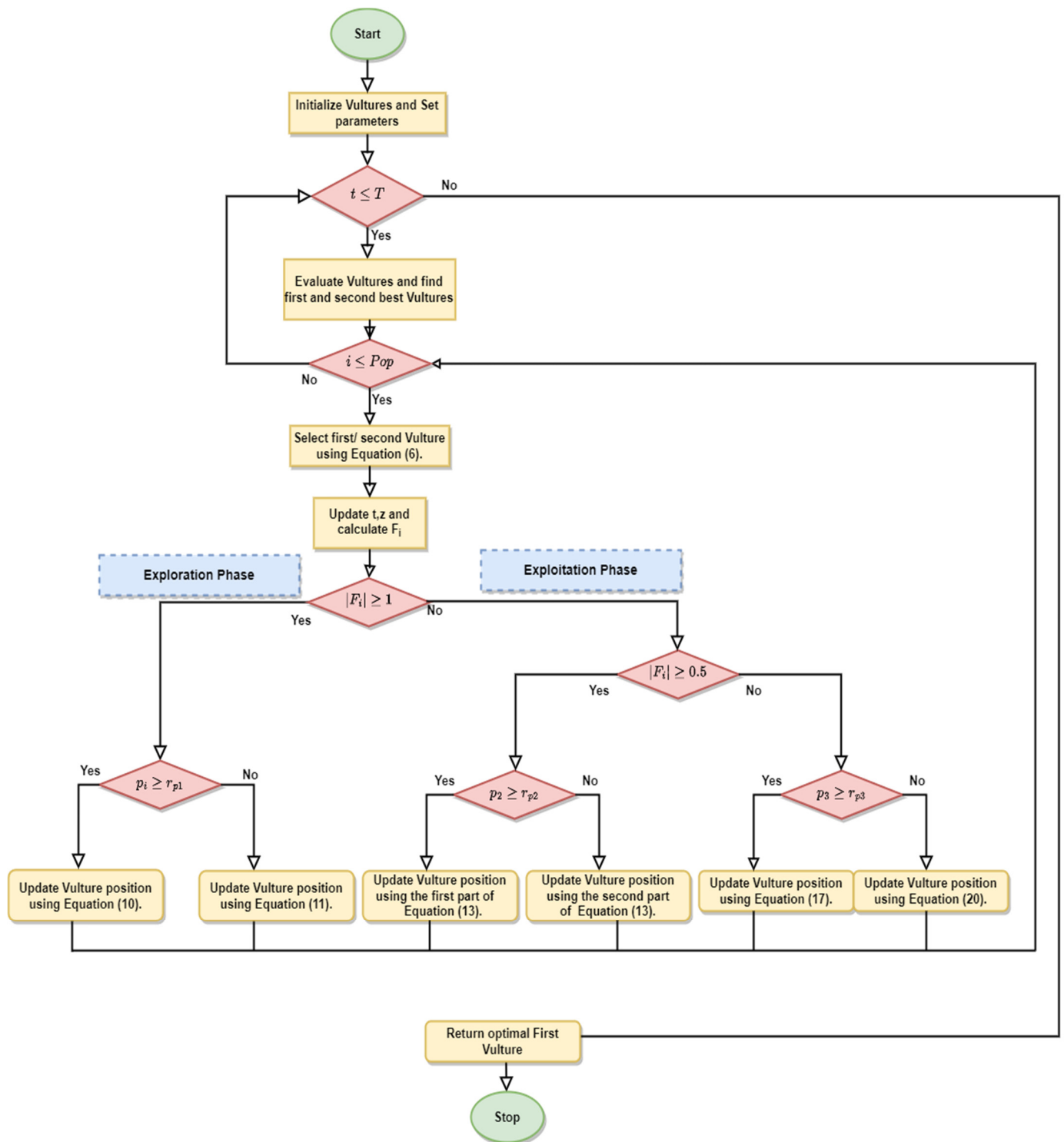


Figure 11. Flowchart of African Vulture Optimization Algorithm.

Here, $BestVulture_1$ represents the best vulture, $BestVulture_2$ denotes the second-best one, L_1 and L_2 are two random values in the range of $[0,1]$ and their total is 1. Equation (7) is used to determine p_i , which was accomplished using the roulette-wheel technique.

$$p_i = \frac{F_i}{\sum_{i=1}^n F_i} \quad (7)$$

Here, the fitness of the first and second two groups of vultures is represented by F_i , and n is the total number of both groups of vultures.

b. Phase 2: The Rate of Starvation of Vultures

If the group of vultures is not starving, they have adequate energy to seek food across larger distances, but if they are starving, they lack the energy to maintain their long-distance flight. As a result, the hungry vultures will have aggressive behavior. The exploration and exploitation stages of vultures may, thus, be constructed based on this behavior. The F_i , a hunger level, of the i th vulture at the t th iteration is computed using Equation (8), which is employed as an indicator of the vultures shift from exploration to exploitation.

$$F_i = (2 \times rand_i + 1) \times z \times \left(1 - \frac{iteration_i}{maxiterations}\right) + t \quad (8)$$

where, F_i indicates that the vultures have had their fill, $rand_i$ is a variable with a random value between 0 and 1, and z is a random value in the range of $[-1,1]$ that changes each iteration, and t is calculated by Equation (9).

$$t = h \times \left(\sin^w \left(\frac{\pi}{2} \times \frac{iteration_i}{maxiterations}\right)\right) + \cos^w \left(\frac{\pi}{2} \times \frac{iteration_i}{maxiterations}\right) - 1 \quad (9)$$

where, the chance of the vulture performing the exploitation stage is determined by the parameter w , which is specified in advance. Moreover, the current iteration number is denoted as $iteration_i$, $maxiterations$ is the total iterations, and h is a random value between -2 and 2 .

F_i will gradually decrease as the number of iterations increases, according to Equation (8). The vultures enter the exploration stage and search for a new food in various locations when the value of $|F_i|$ is larger than 1. Otherwise, vultures go into the exploitation stage, looking for better food in the immediate vicinity.

c. Phase 3: Exploration Stage

The vultures have high visual ability in the natural environment, allowing them to locate food and spot dead creatures quickly. Vultures, however, might have a hard time locating food since they spend a long time examining their surroundings before flying large distances in quest of food. Vultures in the AVOA can inspect various random locations using two distinct strategies, and a parameter named P_1 in the range of $[0,1]$ is utilized to choose either strategy.

To choose one of the strategies during the exploration phase, a random number $rand_{p_1}$ between 0 and 1 is used. Equation (10) is utilized if the value of $rand_{p_1} \leq P_1$ parameter. Otherwise, Equation (11) is utilized.

$$P(i+1) = R(i) - D(i) \times F_i \quad (10)$$

$$P(i+1) = R(i) - F_i + rand_2 \times ((ub - lb) \times rand_3 + lb) \quad (11)$$

Here, $R(i)$ is one of the best vultures chosen in the current iteration using Equation (6), F_i is the current iteration's rate of vulture satiation calculated using Equation (8), $rand_2$ is a random number between 0 and 1, and lb and ub are the variables' lower and upper bounds, respectively. To increase variety and search for different search space areas, $rand_3$ is utilized to provide a high random coefficient at the search environment scale.

Equation (12) calculates $D(i)$, which represents the distance between the vulture and the current optimum one.

$$D(i) = |X \times R(i) - P(i)| \quad (12)$$

Here, $P(i)$ represents the position of the i th vulture, and X is a random value between 0 and 2.

d. Phase 4: Exploitation (First Stage)

At this stage, the AVOA's efficiency stage is explored. The AVOA starts the first stage of exploitation, if $|F_i|$ value is smaller than 1. The parameter P_2 in the range of [0,1] is utilized to decide which strategy is chosen. At the start of this phase, $rand_{p_2}$, a random number between 0 and 1 is produced. The siege-fight strategy is applied slowly if this $rand_{p_2}$ is larger than or equal to the parameter P_2 . Otherwise, the rotational flying technique is used. Equation (13) illustrates this procedure.

$$P(i+1) = \begin{cases} D(i) \times (F_i + rand_4) - d(t) & \text{if } P_2 \geq rand_{p_2} \\ R(i) - (S_1 + S_2) & \text{if } P_2 < rand_{p_2} \end{cases} \quad (13)$$

where, $rand_4$ is a random number between 0 and 1, and $d(t)$ is the distance between the vulture and one of the two groups' best vultures, as computed by Equation (14).

$$d(i) = R(i) - P(i) \quad (14)$$

S_1 and S_2 are calculated using Equations (15) and (16), respectively, as follows:

$$S_1 = R(i) \times \left(\frac{rand_5 \times P(i)}{2\pi} \right) \times \cos(P(i)) \quad (15)$$

$$S_2 = R(i) \times \left(\frac{rand_6 \times P(i)}{2\pi} \right) \times \sin(P(i)) \quad (16)$$

where, $rand_5$ and $rand_6$ are random numbers between 0 and 1, respectively.

e. Phase 5: Exploitation (Second Stage)

This stage of the algorithm is implemented if $|F_i|$ is smaller than 0.5. At the start of this phase, the $rand_3$ is generated in the range of [0,1]. So, if the parameter P_3 is larger than or equal to $rand_3$, the strategy is to attract a variety of vultures to the source of food, resulting in competitive behavior. Therefore, the vulture's position can be updated using Equation (17).

$$P(i+1) = \frac{A_1 + A_2}{2} \quad (17)$$

Equations (18) and (19) are used to calculate A_1 and A_2 , respectively.

$$A_1 = BestVulture_1(i) - \frac{BestVulture_1(i) \times P(i)}{BestVulture_1(i) - (P(i))^2} \times F_i \quad (18)$$

$$A_2 = BestVulture_2(i) - \frac{BestVulture_2(i) \times P(i)}{BestVulture_2(i) - (P(i))^2} \times F_i \quad (19)$$

Likewise, when the AVOA is in its second stage, the vultures would flock to the best vulture to scavenge the remaining food. Therefore, the vultures' position can be updated using Equation (20).

$$P(i+1) = R(i) - |d(t)| \times F_i \times Levy(d) \quad (20)$$

Here, d represents the problem dimensions.

The AVOA's effectiveness was increased by employing Lévy flight (LF) patterns, which were derived using Equation (21).

$$LF(x) = 0.001 \times \frac{u \times \sigma}{|v|^{\frac{1}{\rho}}} \quad (21)$$

$$\sigma = \left(\frac{\Gamma(1+\beta) \times \sin\left(\frac{\pi\beta}{2}\right)}{\Gamma(1+\beta/2) \times \beta \times 2 \times \left(\frac{\beta-1}{2}\right)} \right)^{\frac{1}{\rho}} \quad (22)$$

where, v and u are random numbers between 0 and 1, respectively, and β is a constant number of 1.5.

4. Results and Discussion

MATLAB/Simulink [56] is utilized to perform the optimization and simulation of the proposed hybrid system. Moreover, check its performance when using incremental-conductance-based PI controllers for the MPPT for PV and wind systems as well as tuning the PI controllers using the AVOA and PSO methods. Table 1 illustrates the parameters of these two methods.

Table 1. Parameters of the proposed methods.

Parameter	Method	
	AVOA	PSO
No. of particles/populations	30	30
No. of iterations	100	100
Dimension (No. of variables)	2	2
Control parameters p1, p2, p3	0.6, 0.4, 0.6	—
α	0.8	—
β	0.2	—
γ	2.5	—
Inertia weight (w)	—	0.9–0.4
Cognitive factor (c_1)	—	1.5
Social factor (c_2)	—	1.5

4.1. Optimization Results

The introduced AVOA and PSO methods are employed to determine the optimal values of PI controller gains (K_p and K_i), which are the proportional and integral gains) by minimizing the objective function in Equation (3), in which $e(t) = (V_{pv} - V_{MPPT_{ref}})$ for the PV system before it was coupled to the hybrid system. The $K_{p_{pv}}$ and $K_{i_{pv}}$ values are 125.069 and 12.214, respectively, using the AVOA. The values of $K_{p_{pv}}$ and $K_{i_{pv}}$ in the case of using the PSO method are 152.447 and 13.435, respectively, as shown in Figure 12. Figure 13 illustrates the convergence curves of the ITAE minimization by using the AVOA and PSO method, where the AVOA algorithm takes 9.69 h to converge and achieves a lower ITAE value (0.60574) than the PSO approach, which takes 9.77 h.

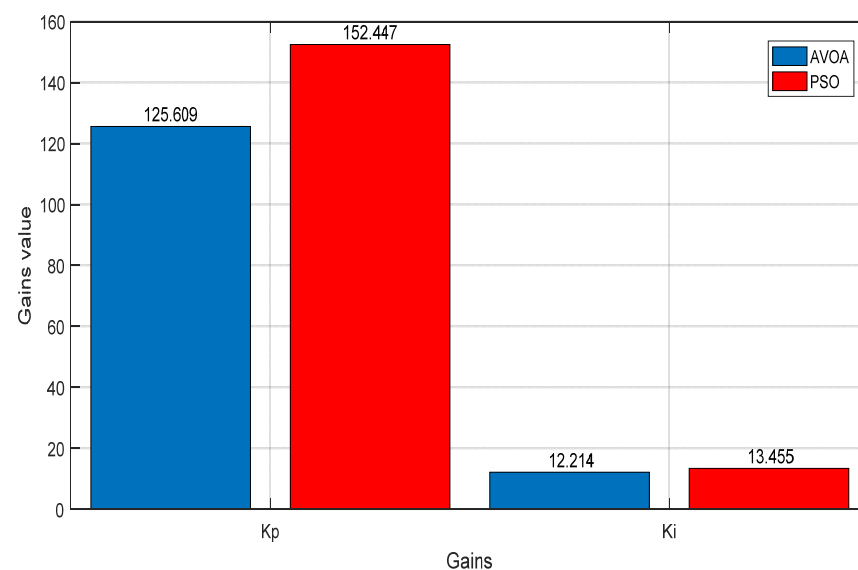


Figure 12. Tuning of PI controllers of the PV system using AVOA and PSO methods.

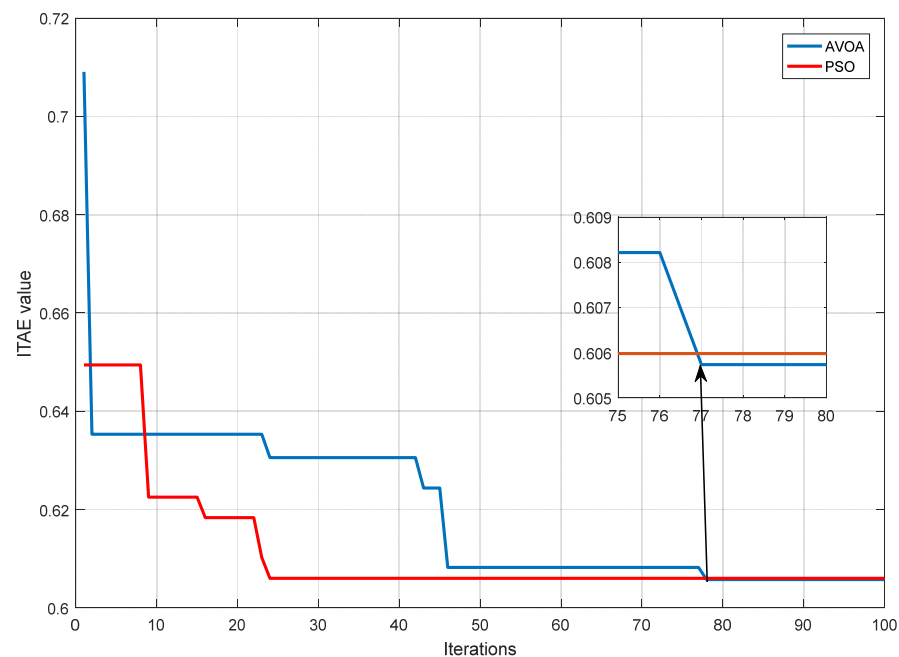


Figure 13. Convergence curves for tuning of PI controllers of the PV system using AVOA and PSO methods.

Moreover, before the wind system was linked to the hybrid system, the AVOA and PSO methods were used to determine the optimal gains of the PI controller in this system by minimizing the objective function in Equation (3), in which $e(t) = (V_{wind_{rectified}} - V_{MPPT_{ref}})$. Using the AVOA method, the $K_{p_{wind}}$ and $K_{i_{wind}}$ values are 2.472 and 70.16, respectively, as shown in Figure 14. The values of $K_{p_{wind}}$ and $K_{i_{wind}}$ using the PSO method are 97.169 and 30.469, respectively. Figure 15 shows that the optimal value of ITAE using the AVOA method is 5.8536, which is substantially better and more accurate than the 9.2697 when using the PSO method. In addition, the AVOA method converges in 6.27 h, which is quicker than the PSO method's 6.37 h.

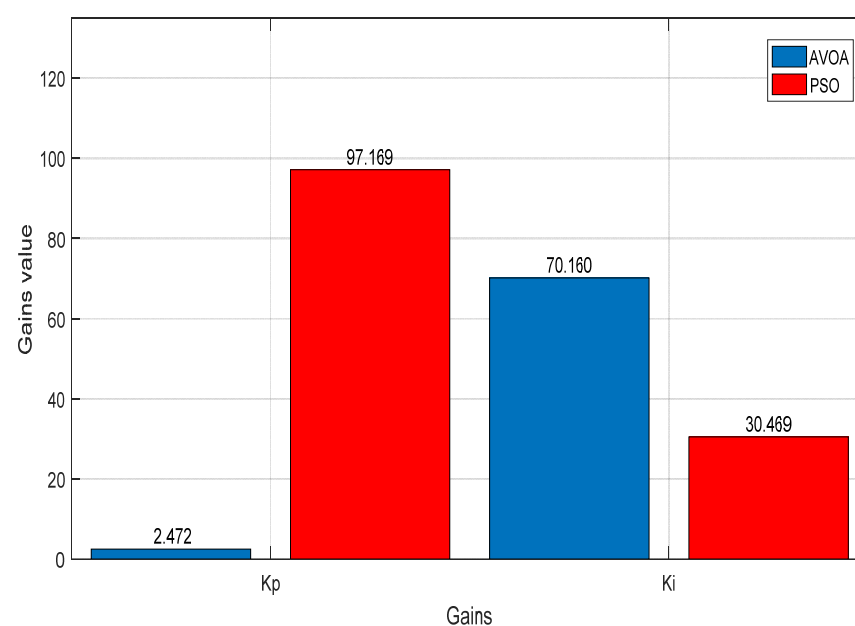


Figure 14. Tuning of PI controllers in the wind system using AVOA and PSO methods.

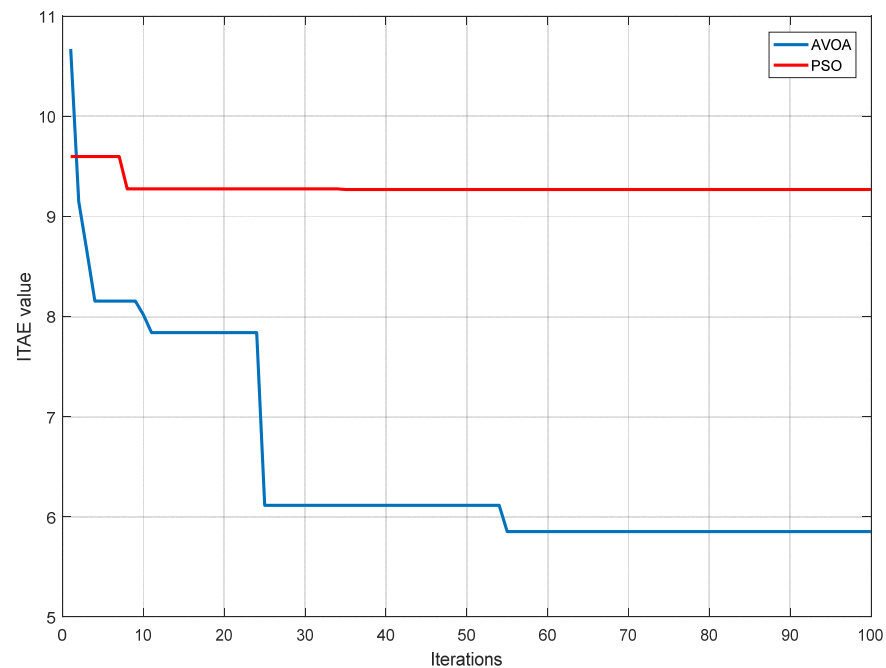


Figure 15. Convergence curves for tuning of PI controllers in the wind system using AVOA and PSO methods.

In the storage system, the AVOA and PSO methods were also applied for tuning the PI controller's optimal gains, by minimizing the objective function in Equation (3) in which $e(t) = ((I_{bat} - I_{charge_{ref}}) + (I_{bat} - I_{discharge_{ref}}))$, before this system was linked to the hybrid system. When employing the AVOA method, the $K_{p1_{bat}}$, $K_{i1_{bat}}$, $K_{p2_{bat}}$, $K_{i2_{bat}}$ values are 200, 0.107, 200, and 148.15, respectively, as shown in Figure 16. Whereas the obtained values of the $K_{p1_{bat}}$, $K_{i1_{bat}}$, $K_{p2_{bat}}$, and $K_{i2_{bat}}$ using the PSO method are 125.314, 1, 117.2, and 57.435, respectively. Figure 17 shows that the optimal value of ITAE using the AVOA method is 0.51989, which is better and more accurate than the value obtained using the PSO method, which is 0.52132. In addition, the AVOA method takes 5.04 h to converge, whereas the PSO method takes 5.12 h.

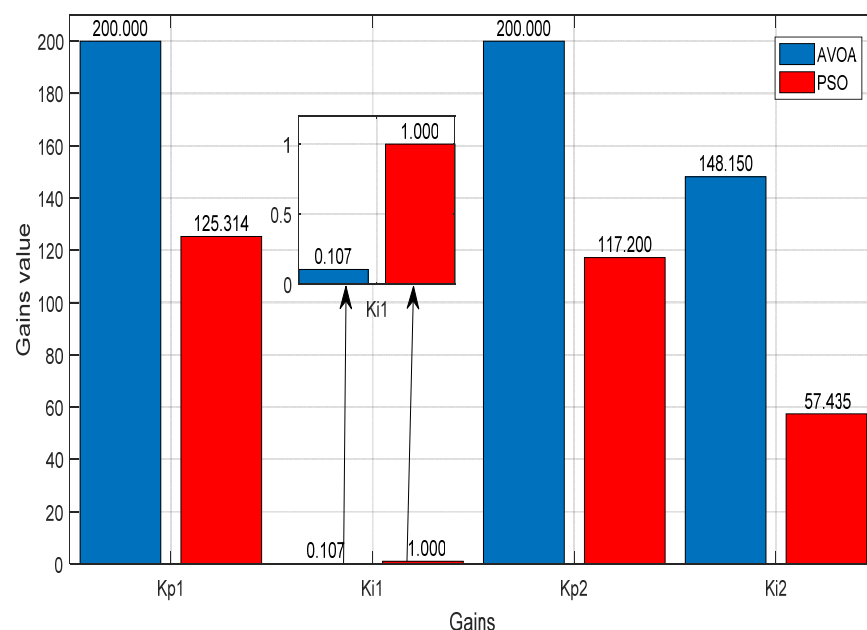


Figure 16. Tuning of PI controllers in the storage system using AVOA and PSO methods.

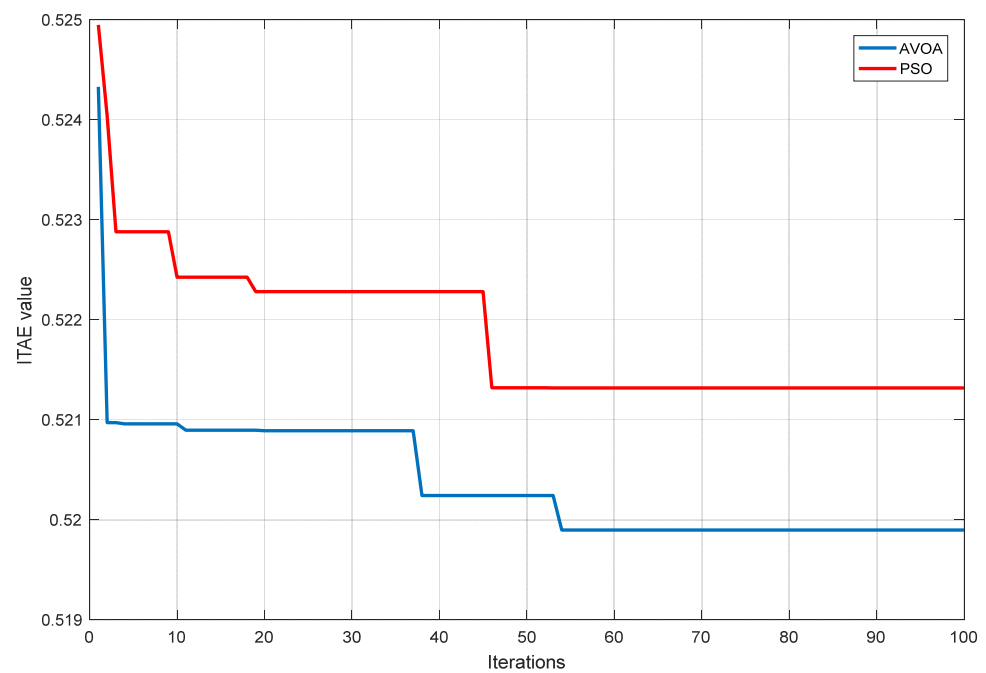


Figure 17. Convergence curves for tuning of PI controllers in the storage system using AVOA and PSO methods.

4.2. Simulation Results

The hybrid system's performance was evaluated in this part after optimal tuning of the PI controllers using the AVOA and PSO methods. To prevent the output voltage of the wind system from fluctuating and making the DC bus voltage 500 V, the reference voltage of the VSC was raised to 503.5 V in the AC system, as illustrated in Figure 18. In this AC system, it was required to supply the DC load by 100 kW. Figure 19 depicts the system's total power plus losses, which are roughly 4.0355 kW using the AVOA method and 4.0435 kW using the PSO technique.

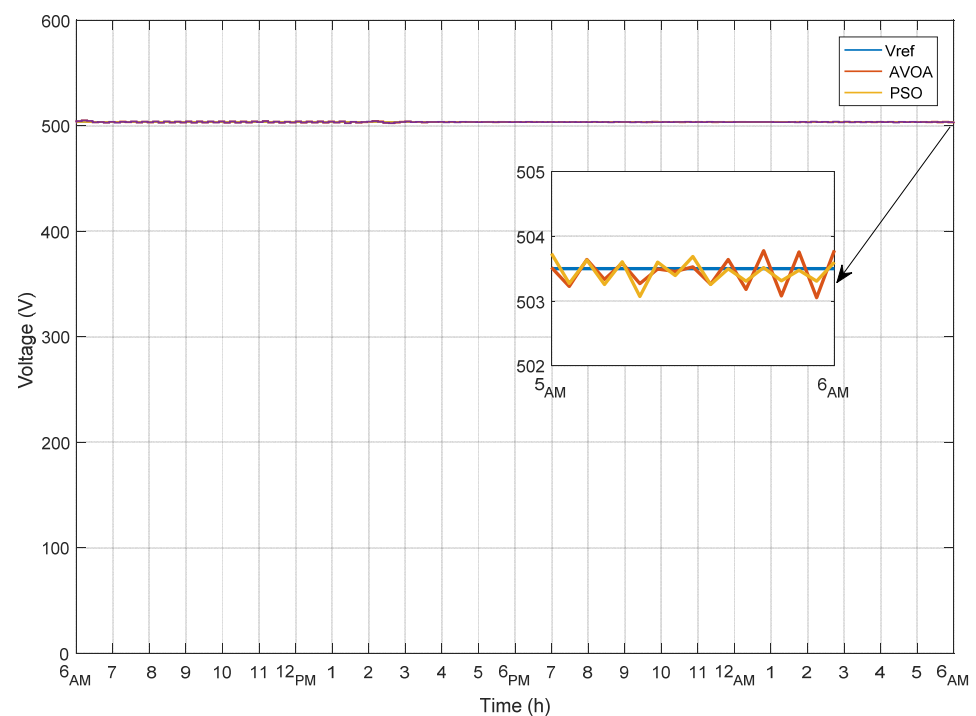


Figure 18. Output DC voltage of the AC system.

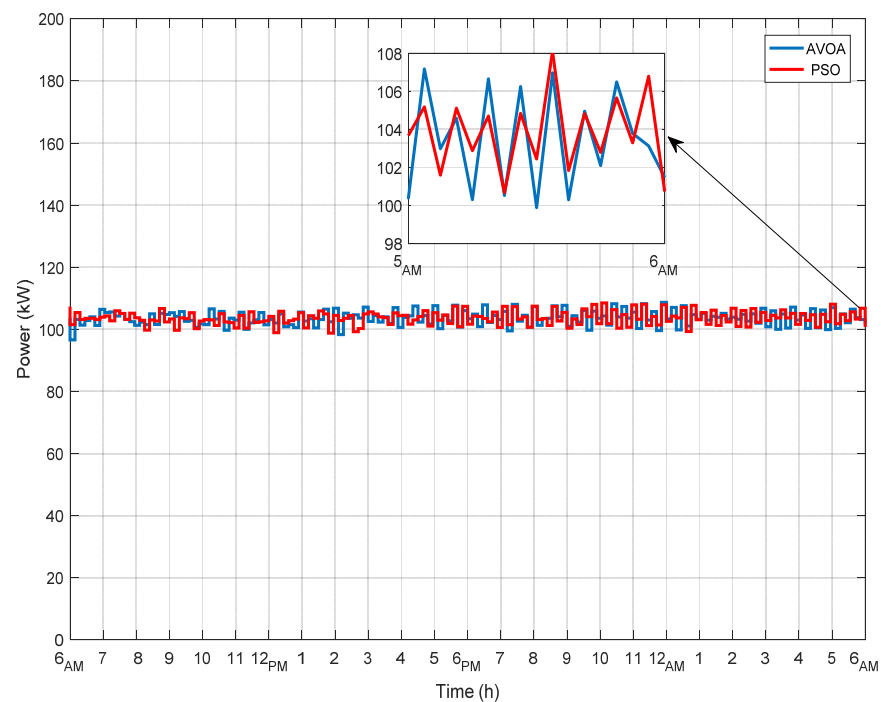


Figure 19. Power generated from the AC system.

Second, in the PV system, the incremental conductance based on a PI controller, where the reference voltage is generated, is utilized to track the MPP. The error between the PV array's voltage and this reference voltage is minimized using a PI controller that is tuned using the AVOA and PSO methods. The PV array's voltage as well as this reference voltage, by those methods, are shown in Figure 20. The output or boosted voltage of this system is 500 V, as shown in Figure 21, which also represents the hybrid system's DC bus voltage. The PV system was modeled to supply the DC load with 20 kW. Figure 22 shows the power generated from the PV system in which the MPP was, moving according to the input irradiance, tracked using the incremental conductance based on a PI controller that produces the firing pulses to the boost converter.

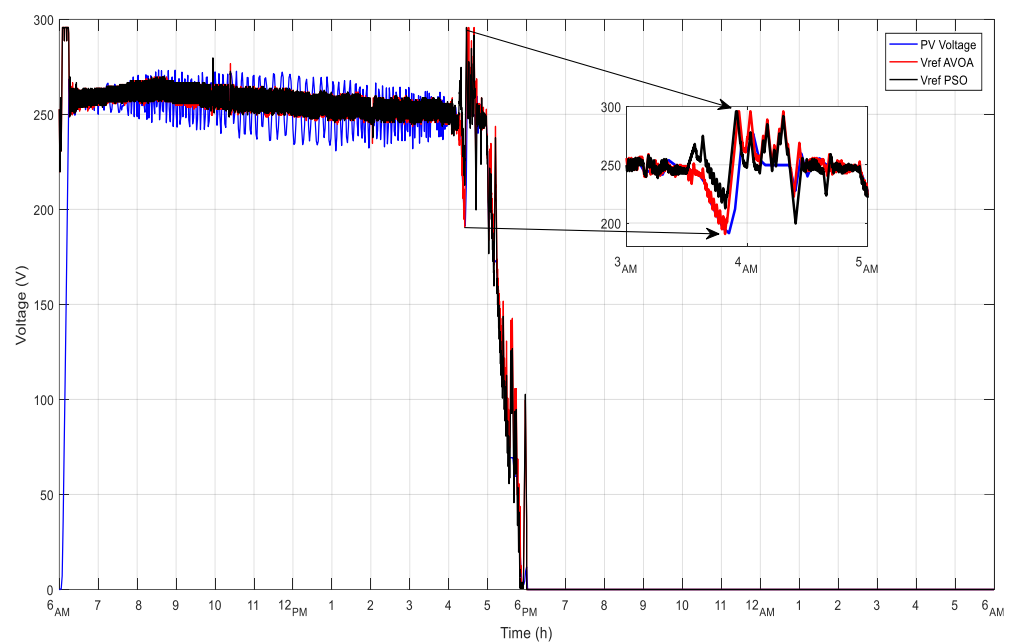


Figure 20. PV array and reference voltages in the PV system.

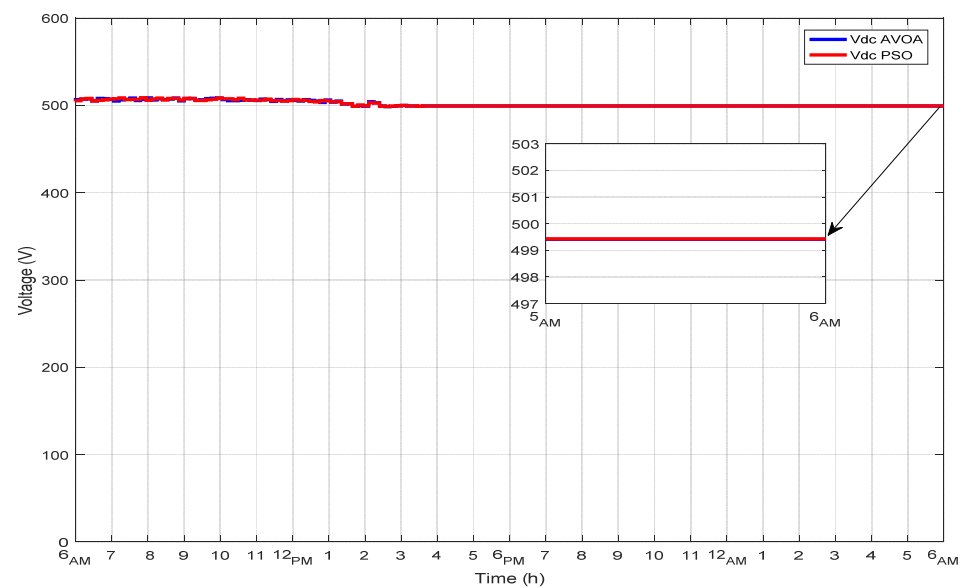


Figure 21. DC bus voltage.

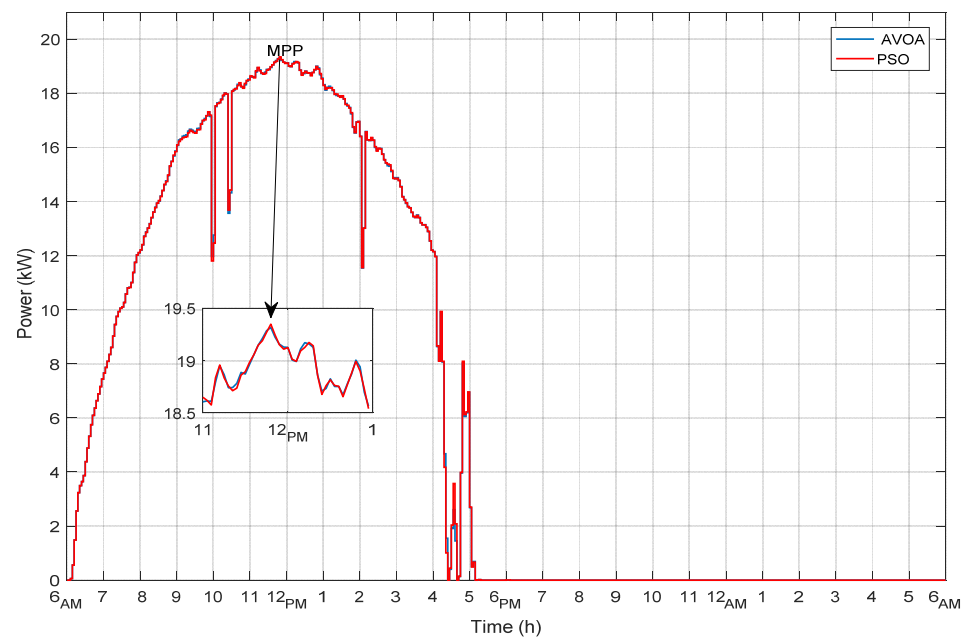


Figure 22. Power with MPP of the PV system.

Third, in the wind system, the speed of the synchronous generator is almost at unity, using both the AVOA and PSO methods, as shown in Figure 23, despite the fluctuations in the wind speed, as shown in Figure 8. In the same manner of the PV system, the incremental-conductance method based on the PI controller is applied to follow the MPP in which the reference voltage is generated, except that the incremental conductance's inputs are the rectified voltage and current. The error between the rectified and reference voltages was also minimized using the tuned PI controller. The rectified voltage as well as this reference voltage obtained by the AVOA and PSO methods are shown in Figure 24. The wind system was also modeled to supply the DC load with 10 kW. Figure 25 shows the power generated from the wind system in which the MPP was tracked using the incremental conductance based on the PI controller, which produced the firing pulses to the boost converter in the system.

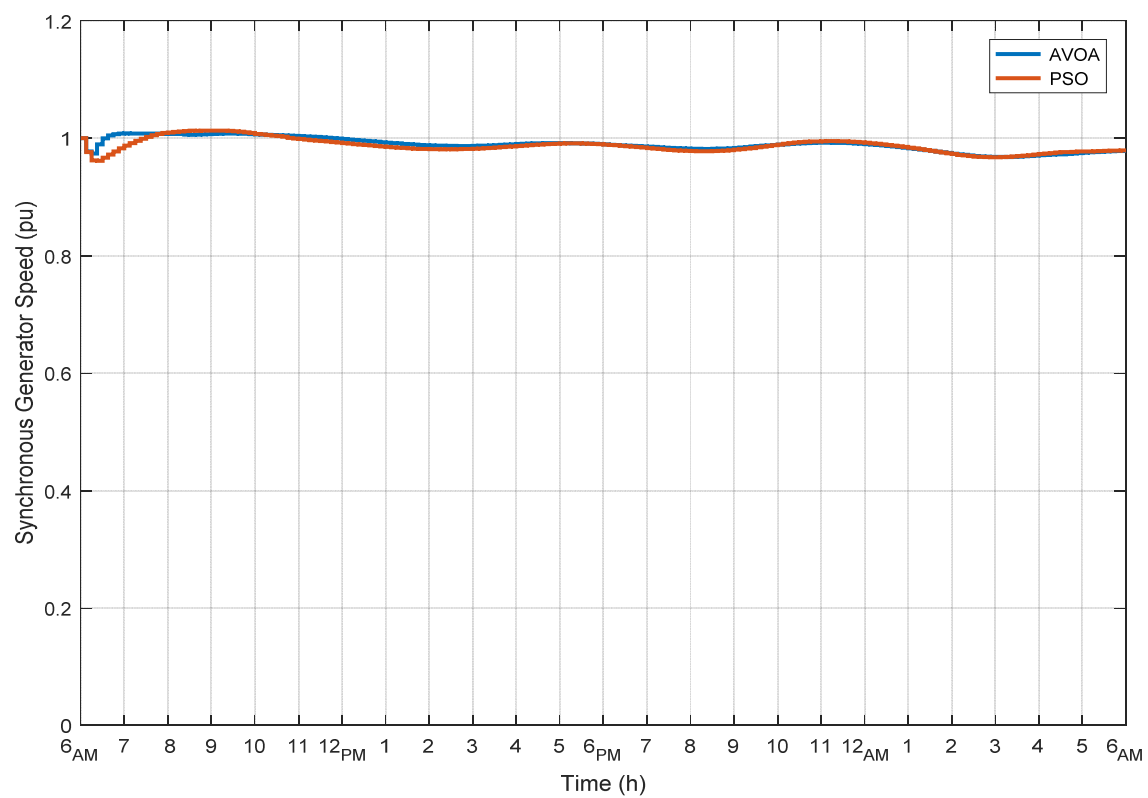


Figure 23. Speed of synchronous generator in p.u.

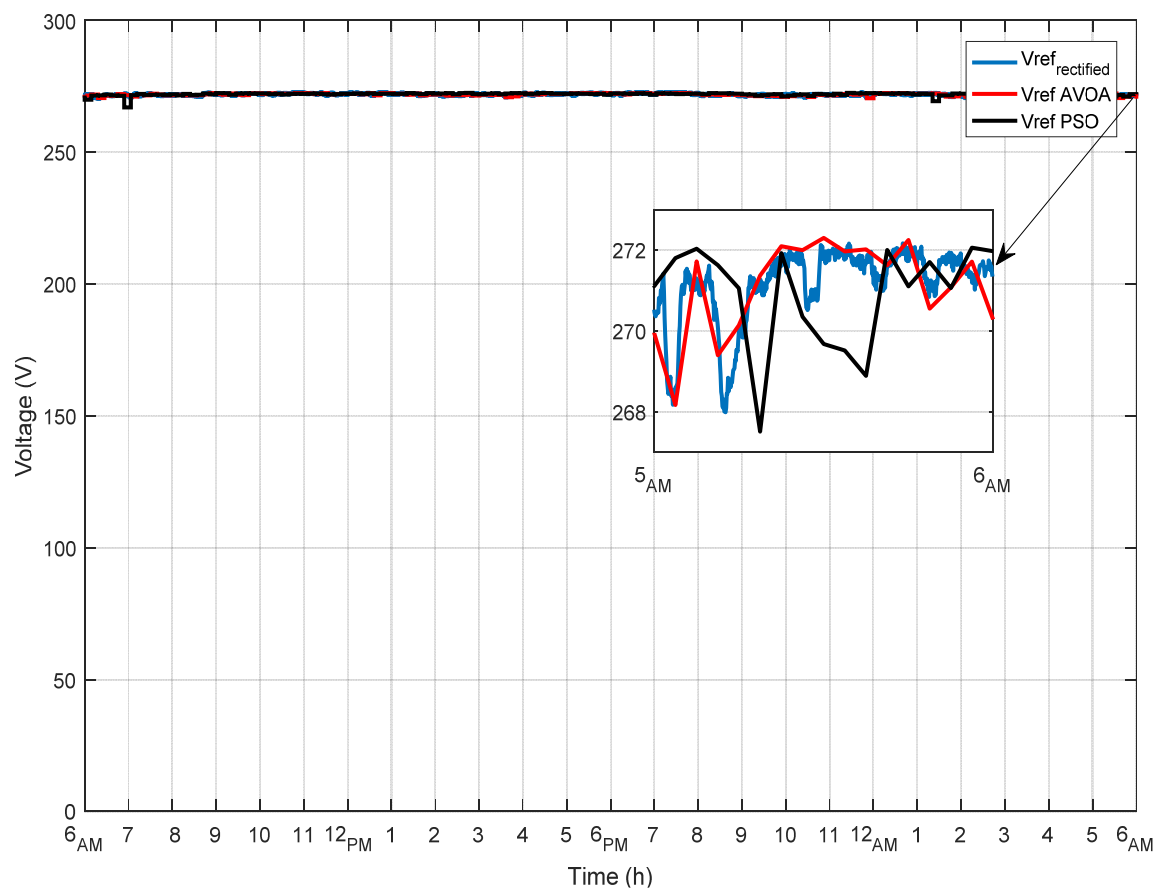


Figure 24. Rectified and reference voltages in the wind system.

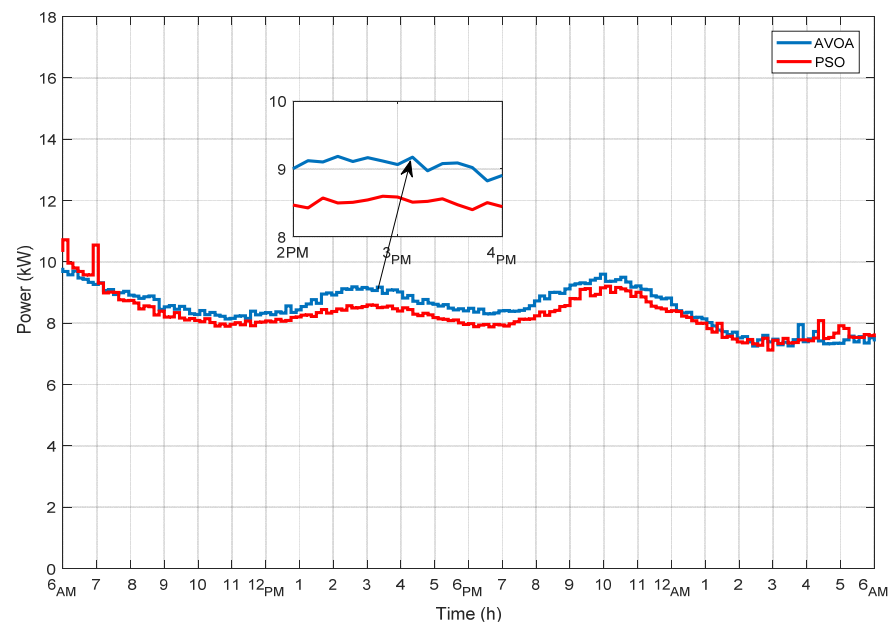


Figure 25. Power generated from the wind system.

Fourth, in the storage system, a bi-directional buck-boost converter is employed to charge and discharge the battery in response to fluctuations in the output of PV and wind systems. These systems are designed to provide 30 kW of DC power. Nevertheless, due to the irregular nature of wind speed and solar irradiance, this much power cannot be fully supplied or both systems would supply more power than what is required, so the buck-boost converter is utilized to control the power generated by the renewable-energy systems as well as the power supplied by this storage system, to provide the DC load with power of 30 kW, as shown in Figure 26. Moreover, the total DC load delivered by the proposed hybrid system is 130 kW, as illustrated in Figure 27.

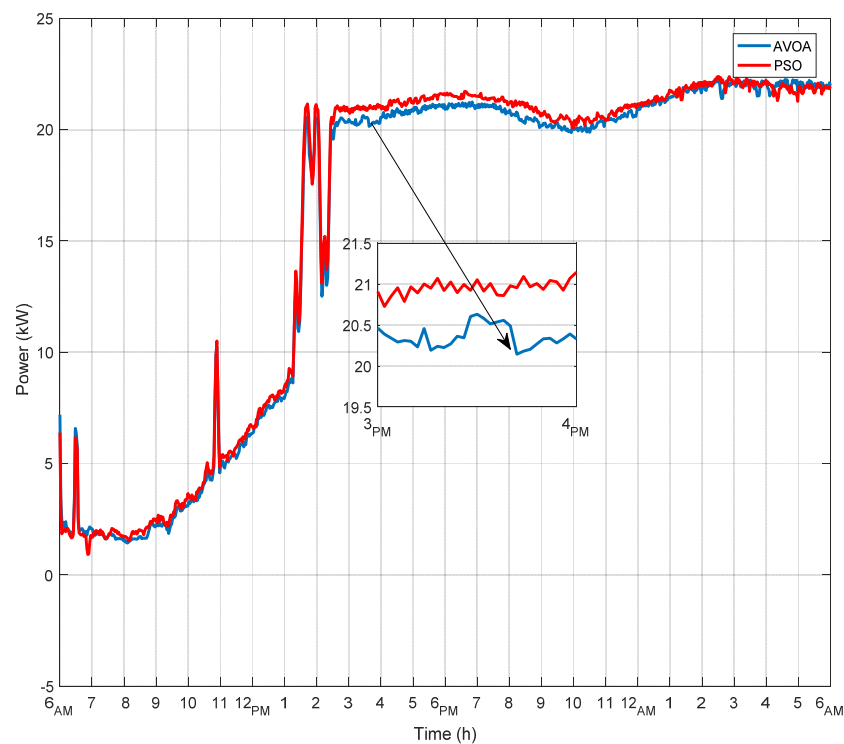


Figure 26. Power supplied from the storage system.

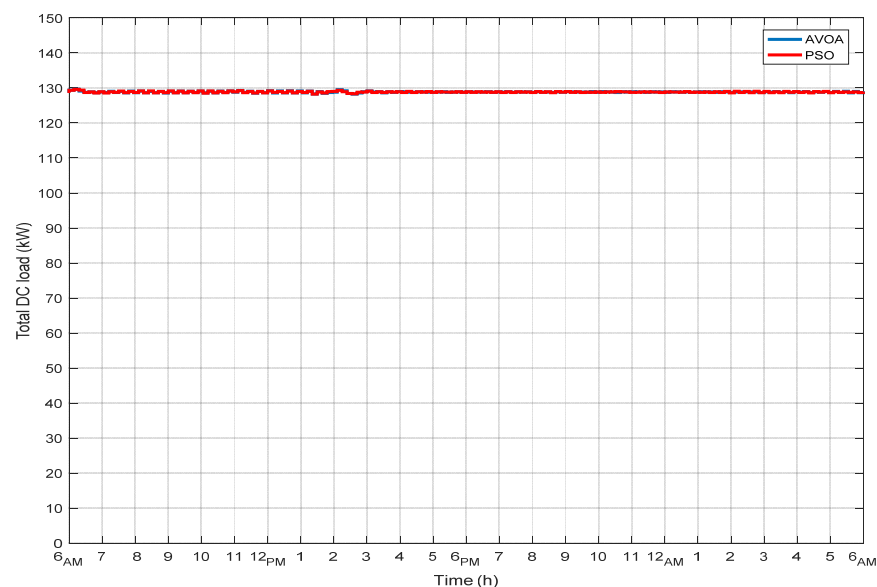


Figure 27. Total DC load supplied from the hybrid system.

5. Conclusions

In this work, a novel optimization algorithm (the AVOA) is utilized to tune the PI controllers to improve the performance of a 130-kW grid-connected hybrid system. The main purpose of this work is to achieve the MPP of renewable-energy (PV and wind) systems. Moreover, the optimal tuning of the PI controllers to reduce the error between the generated voltage by such systems and the reference voltage was obtained by the MPPT controllers. The AVOA is employed to the fitness function, which is composed of the integral of the system variables' time multiplied by the absolute error. The optimization results have demonstrated the superiority and high performance of the proposed AVOA method. Moreover, the simulation of the hybrid system shows competitive results, as compared to the PSO technique. Furthermore, the obtained results of this system have given an improvement of more than 3% in reducing the power supplied from the storage system, which indicates that the extracted power from RESs using the AVOA method is better than the PSO method. In addition to its prior success in other industrial-optimization fields, the AVOA algorithm can be concluded to be a competitive metaheuristic approach to tuning numerous PI controllers in a grid-connected renewable-energy system. Though some challenges were faced in the optimization of the PI controllers in the proposed hybrid system as a whole, which posed a big issue. As a result, the optimization for these controllers was done for each system, i.e., the PV, wind, and storage systems individually. Moreover, the modeling of the bi-directional buck-boost converter is another difficulty, since it is needed for charging and discharging the storage battery, according to the output fluctuations of PV and wind systems. Therefore, it is recommended for further work to be done on the optimization at a workstation computer with higher specifications. In addition, it is recommended to investigate this system as the penetration level of RESs increases as a trend for further work.

Author Contributions: Funding acquisition, W.K., S.P. and H.-J.C.; investigation, G.A.G., H.M.H. and E.A.A.-A.; methodology, G.A.G.; resources, W.K., S.P. and H.-J.C.; software, G.A.G.; supervision, E.A.A.-A.; writing—original draft, G.A.G.; writing—review and editing, H.M.H. and R.A.T. All authors have read and agreed to the published version of the manuscript.

Funding: Energy Technology Development Project of Korea Institute of Energy Technology Evaluation and Planning (KETEP): 20192010106990.

Institutional Review Board Statement: Not applicable.

Informed Consent Statement: Not applicable.

Data Availability Statement: Not applicable.

Acknowledgments: This work was a project to support the energy technology development program of the Korea Institute of Energy Technology Evaluation (KETEP) supported by the Ministry of Trade, Industry and Energy (No. 2010106990).

Conflicts of Interest: The authors declare no conflict of interest.

Appendix A

The data of the hybrid renewable-energy system under study are listed in the following tables.

Table A1. Data of AC system.

AC-Generator Ratings	
Line-to-line voltage	25 kV
Frequency	60 Hz
Base power	50 MVA
Base voltage	25 kV
X/R ratio	7
Transformer ratings	
Nominal power	111.11 kVA
Primary voltage	25 kV
Secondary voltage	380 V
Frequency	60 Hz
Universal Bridge (IGBT) ratings	
Snubber-resistance R_s	100 k Ω
Snubber-capacitance C_s	inf
R_{on}, L_{on}	1 m Ω , 0 H
Forward voltage (V_f)	0 V

Table A2. Data of PV module.

Parameter	Rating
Module type	Tata Power Systems TP240MBZ
Maximum power (P_m)	238.95 W
Number of cells	60
Open-circuit voltage (V_{oc})	36.5 V
Max-power voltage (V_{mp})	29.5 V
Short-circuit current (I_{sc})	8.78 A
Max-power current (I_{mp})	8.1 A
Series resistance (R_s)	0.32793 Ω
Shunt resistance (R_{sh})	113.1517 Ω
Voltage-temp. coefficient	−0.33 (%V/°C)
Current-temp. coefficient	0.063804 (%/°C)

Table A3. Data of DC–DC boost converter.

Parameter	Rating
Input DC Voltage	253.7 V
Output DC Voltage	500 V
Switching frequency	5 kHz
L	1.6 mH
C_{pv}	1.6 mF
C_{out}	12 mF

Table A4. Data of wind system.

Wind Turbine	
Nominal mechanical-output power	10 (kW)
Wind speed at nominal speed	11 (m/s)
2-Mass Drive Train	
Wind-turbine inertia constant H	4.32 (s)
Shaft-spring constant	0.3 (p.u.)
Shaft mutual damping	1.5 (p.u.)
Turbine initial speed	1 (p.u.)
Initial output torque	1 (p.u.)
Synchronous generator ratings	
Power	11.11 kVA
Frequency	60 Hz
Line to line voltage	220 V
Reactances [X_d , X_d' , X_d'' , X_q , X_q''] in p.u.	[1.305, 0.296, 0.252, 0.474, 0.243]
Time constants [T_d' , T_d'' , T_q''] in seconds	[4.49, 0.0681, 0.0513]
Inertia constant H (s), friction factor F (p.u.), and pairs of poles	[0.62, 0.01, 4]
Rectifier (Diodes)	
Snubber-resistance R_s	0.15 Ω
Snubber-capacitance C_s	0.55 μ F
R_{on} , L_{on}	1 $\mu\Omega$, 0 H
Forward voltage (V_f)	0 V

Table A5. Data of storage system.

Parameter	Rating
Type	Lithium-Ion
Nominal voltage	120 V
Rated capacity	800 Ah
Initial state of charge	50 %
Buck-boost-converter ratings	
C_{in}	1.6 mF
C_{out}	12 mF
L	0.3 mH
Diodes of buck-boost converter	
Internal resistance (R_{on})	1 m Ω
Snubber resistance (R_s)	100 k Ω
Snubber capacitance (C_s)	Inf

Table A6. Data of electric loads.

Parameter	Rating
DC-bus voltage	500 V
Load ₁ (R_1)	5 Ω
Load ₂ (R_2)	6.25 Ω
Load ₃ (R_3)	8.33 Ω
Load ₄ (R_4)	25 Ω

References

1. Ahmad, R.; Murtaza, A.F.; Sher, H.A. Power tracking techniques for efficient operation of photovoltaic array in solar applications—A review. *Renew. Sustain. Energy Rev.* **2019**, *101*, 82–102. [\[CrossRef\]](#)
2. Mohamed, M.A.; Diab, A.A.Z.; Rezk, H. Partial shading mitigation of PV systems via different meta-heuristic techniques. *Renew. Energy* **2019**, *130*, 1159–1175. [\[CrossRef\]](#)
3. Lotfi, H.; Khodaei, A. AC versus DC microgrid planning. *IEEE Trans. Smart Grid* **2017**, *8*, 296–304. [\[CrossRef\]](#)
4. Zakir, M.; Sher, H.A.; Arshad, A.; Lehtonen, M. A fault detection, localization, and categorization method for PV fed DC-microgrid with power-sharing management among the nano-grids. *Int. J. Electr. Power Energy Syst.* **2022**, *137*, 107858. [\[CrossRef\]](#)
5. Raiker, G.A.; Loganathan, U. Current control of boost converter for PV interface with momentum-based perturb and observe MPPT. *IEEE Trans. Ind. Appl.* **2021**, *57*, 4071–4079. [\[CrossRef\]](#)
6. Jatelly, V.; Azzopardi, B.; Joshi, J.; Sharma, A.; Arora, S. Experimental analysis of hill-climbing MPPT algorithms under low irradiance levels. *Renew. Sustain. Energy Rev.* **2021**, *150*, 111467. [\[CrossRef\]](#)
7. Ali, M.N.; Mahmoud, K.; Lehtonen, M.; Darwish, M.M. An efficient fuzzy-logic based variable-step incremental conductance MPPT method for grid-connected PV systems. *IEEE Access* **2021**, *9*, 26420–26430. [\[CrossRef\]](#)
8. Nadeem, A.; Sher, H.A.; Murtaza, A.F. Online fractional open-circuit voltage maximum output power algorithm for photovoltaic modules. *IET Renew. Power Gener.* **2020**, *14*, 188–198. [\[CrossRef\]](#)
9. Nadeem, A.; Sher, H.A.; Murtaza, A.F.; Ahmed, N. Online current-sensorless estimator for PV open circuit voltage and short circuit current. *Sol. Energy* **2021**, *213*, 198–210. [\[CrossRef\]](#)
10. Fathi, M.; Parian, J.A. Intelligent MPPT for photovoltaic panels using a novel fuzzy logic and artificial neural networks based on evolutionary algorithms. *Energy Rep.* **2021**, *7*, 1338–1348. [\[CrossRef\]](#)
11. Dehghani, M.; Taghipour, M.; Gharehpetian, G.B.; Abedi, M. Optimized fuzzy controller for MPPT of grid-connected PV systems in rapidly changing atmospheric conditions. *J. Mod. Power Syst. Clean Energy* **2020**, *9*, 376–383. [\[CrossRef\]](#)
12. Eltamaly, A.M.; Al-Saud, M.S.; Abokhalil, A.G.; Farh, H.M. Simulation and experimental validation of fast adaptive particle swarm optimization strategy for photovoltaic global peak tracker under dynamic partial shading. *Renew. Sustain. Energy Rev.* **2020**, *124*, 109719. [\[CrossRef\]](#)
13. Pilakkat, D.; Kanthalakshmi, S. An improved P&O algorithm integrated with artificial bee colony for photovoltaic systems under partial shading conditions. *Sol. Energy* **2019**, *178*, 37–47.
14. Guo, K.; Cui, L.; Mao, M.; Zhou, L.; Zhang, Q. An improved gray wolf optimizer MPPT algorithm for PV system with BFBIC converter under partial shading. *IEEE Access* **2020**, *8*, 103476–103490. [\[CrossRef\]](#)
15. Huang, Y.P.; Huang, M.Y.; Ye, C.E. A fusion firefly algorithm with simplified propagation for photovoltaic MPPT under partial shading conditions. *IEEE Trans. Sustain. Energy* **2020**, *11*, 2641–2652. [\[CrossRef\]](#)
16. Jamaludin, M.N.I.; Tajuddin, M.F.N.; Ahmed, J.; Azmi, A.; Azmi, S.A.; Ghazali, N.H.; Alhelou, H.H. An effective salp swarm based MPPT for photovoltaic systems under dynamic and partial shading conditions. *IEEE Access* **2021**, *9*, 34570–34589. [\[CrossRef\]](#)
17. Phanden, R.K.; Sharma, L.; Chhabra, J.; Demir, H.I. A novel modified ant colony optimization based maximum power point tracking controller for photovoltaic systems. *Mater. Today Proc.* **2021**, *38*, 89–93. [\[CrossRef\]](#)
18. Mosaad, M.I.; abed el-Raouf, M.O.; Al-Ahmar, M.A.; Banakher, F.A. Maximum power point tracking of PV system based cuckoo search algorithm; review and comparison. *Energy Procedia* **2019**, *162*, 117–126. [\[CrossRef\]](#)
19. Charin, C.; Ishak, D.; Zainuri, M.A.A.M.; Ismail, B.; Jamil, M.K.M. A hybrid of bio-inspired algorithm based on Levy flight and particle swarm optimizations for photovoltaic system under partial shading conditions. *Sol. Energy* **2021**, *217*, 1–14. [\[CrossRef\]](#)
20. Kumar, R.; Agrawal, H.P.; Shah, A.; Bansal, H.O. Maximum power point tracking in wind energy conversion system using radial basis function based neural network control strategy. *Sustain. Energy Technol. Assess.* **2019**, *36*, 100533. [\[CrossRef\]](#)
21. Fathy, A.; El-baksawi, O. Grasshopper optimization algorithm for extracting maximum power from wind turbine installed in Al-Jouf region. *J. Renew. Sustain. Energy* **2019**, *11*, 033303. [\[CrossRef\]](#)
22. El Yaakoubi, A.; Attari, K.; Asselman, A.; Djebli, A. Novel power capture optimization based sensorless maximum power point tracking strategy and internal model controller for wind turbines systems driven SCIG. *Front. Energy* **2019**, *13*, 742–756. [\[CrossRef\]](#)
23. Karabacak, M. A new perturb and observe based higher order sliding mode MPPT control of wind turbines eliminating the rotor inertial effect. *Renew. Energy* **2019**, *133*, 807–827. [\[CrossRef\]](#)
24. Fathy, A.; Alharbi, A.G.; Alshammari, S.; Hasani, H.M. Archimedes optimization algorithm based maximum power point tracker for wind energy generation system. *Ain Shams Eng. J.* **2022**, *13*, 101548. [\[CrossRef\]](#)
25. Balbino, A.J.; Nora, B.D.S.; Lazzarin, T.B. An Improved Mechanical Sensorless Maximum Power Point Tracking Method for Permanent-Magnet Synchronous Generator-Based Small Wind Turbines Systems. *IEEE Trans. Ind. Electron.* **2021**, *69*, 4765–4775. [\[CrossRef\]](#)
26. Haq, I.U.; Khan, Q.; Khan, I.; Akmeliawati, R.; Nisar, K.S.; Khan, I. Maximum power extraction strategy for variable speed wind turbine system via neuro-adaptive generalized global sliding mode controller. *IEEE Access* **2022**, *8*, 128536–128547. [\[CrossRef\]](#)
27. Khan, M.J. An AIAPPO MPPT controller based real time adaptive maximum power point tracking technique for wind turbine system. *ISA Trans.* **2022**, *123*, 492–504. [\[CrossRef\]](#)
28. Huynh, P.; Tungare, S.; Banerjee, A. Maximum power point tracking for wind turbine using integrated generator–rectifier systems. *IEEE Trans. Power Electron.* **2020**, *36*, 504–512. [\[CrossRef\]](#)

29. Lamsal, D.; Sreeram, V.; Mishra, Y.; Kumar, D. Smoothing control strategy of wind and photovoltaic output power fluctuation by considering the state of health of battery energy storage system. *IET Renew. Power Gener.* **2019**, *13*, 578–586. [\[CrossRef\]](#)
30. Mostafa, M.R.; Saad, N.H.; El-sattar, A.A. Tracking the maximum power point of PV array by sliding mode control method. *Ain Shams Eng. J.* **2020**, *11*, 119–131. [\[CrossRef\]](#)
31. Merchaoui, M.; Hamouda, M.; Sakly, A.; Mimouni, M.F. Fuzzy logic adaptive particle swarm optimisation based MPPT controller for photovoltaic systems. *IET Renew. Power Gener.* **2020**, *14*, 2933–2945. [\[CrossRef\]](#)
32. Awais, M.; Khan, L.; Ahmad, S.; Mumtaz, S.; Badar, R. Nonlinear adaptive Neuro Fuzzy feedback linearization based MPPT control schemes for photovoltaic system in microgrid. *PLoS ONE* **2020**, *15*, e0234992. [\[CrossRef\]](#) [\[PubMed\]](#)
33. Sibtain, D.; Murtaza, A.F.; Ahmed, N.; Sher, H.A.; Gulzar, M.M. Multi control adaptive fractional order PID control approach for PV/wind connected grid system. *Int. Trans. Electr. Energy Syst.* **2021**, *31*, e12809. [\[CrossRef\]](#)
34. Martinez-Lopez, M.; Moreno-Valenzuela, J.; He, W. A robust nonlinear PI-type controller for the DC–DC buck–boost power converter. *ISA Trans.* **2022**. [\[CrossRef\]](#)
35. Hasanien, H.M.; Mueen, S.M. Design optimization of controller parameters used in variable speed wind energy conversion system by genetic algorithms. *IEEE Trans. Sustain. Energy* **2012**, *3*, 200–208. [\[CrossRef\]](#)
36. Qais, M.H.; Hasanien, H.M.; Alghuwainem, S. Augmented grey wolf optimizer for grid-connected PMSG-based wind energy conversion systems. *Appl. Soft Comput.* **2018**, *69*, 504–515. [\[CrossRef\]](#)
37. Hasanien, H.M. Performance improvement of photovoltaic power systems using an optimal control strategy based on whale optimization algorithm. *Electr. Power Syst. Res.* **2018**, *157*, 168–176. [\[CrossRef\]](#)
38. Zambrana-Lopez, P.; Fernández-Quijano, J.; Fernandez-Lozano, J.J.; Garcia-Cerezo, A.; Rubio, P.M.M. Fuzzy logic tuning of a PI controller to improve the performance of a wind turbine on a semi-submersible platform under different wind scenarios. *IFAC Pap.* **2020**, *53*, 12364–12371. [\[CrossRef\]](#)
39. Ustun, S.V.; Demirtas, M. Optimal tuning of PI coefficients by using fuzzy-genetic for V/f controlled induction motor. *Expert Syst. Appl.* **2008**, *34*, 2714–2720. [\[CrossRef\]](#)
40. Sahu, R.K.; Panda, S.; Sekhar, G.C. A novel hybrid PSO-PS optimized fuzzy PI controller for AGC in multi area interconnected power systems. *Int. J. Electr. Power Energy Syst.* **2015**, *64*, 880–893. [\[CrossRef\]](#)
41. Abedini, M.; Mahmodi, E.; Mousavi, M.; Chaharmahali, I. A novel Fuzzy PI controller for improving autonomous network by considering uncertainty. *Sustain. Energy Grids Netw.* **2019**, *18*, 100200. [\[CrossRef\]](#)
42. Kalaam, R.N.; Mueen, S.M.; Al-Durra, A.; Hasanien, H.M.; Al-Wahedi, K. Optimisation of controller parameters for grid-tied photovoltaic system at faulty network using artificial neural network-based cuckoo search algorithm. *IET Renew. Power Gener.* **2017**, *11*, 1517–1526. [\[CrossRef\]](#)
43. Zhao, J.; Lin, M.; Xu, D.; Hao, L.; Zhang, W. Vector control of a hybrid axial field flux-switching permanent magnet machine based on particle swarm optimization. *IEEE Trans. Magn.* **2015**, *51*, 1–4.
44. Costa, B.L.G.; Bacon, V.D.; da Silva, S.A.O.; Angélico, B.A. Tuning of a PI-MR controller based on differential evolution metaheuristic applied to the current control loop of a shunt-APF. *IEEE Trans. Ind. Electron.* **2017**, *64*, 4751–4761. [\[CrossRef\]](#)
45. Wang, Y.; Li, S.; Sun, H.; Huang, C.; Youssefi, N. The utilization of adaptive African vulture optimizer for optimal parameter identification of SOFC. *Energy Rep.* **2022**, *8*, 551–560. [\[CrossRef\]](#)
46. Chen, Y.; Zhang, G. New parameters identification of Proton exchange membrane fuel cell stacks based on an improved version of African vulture optimization algorithm. *Energy Rep.* **2022**, *8*, 3030–3040. [\[CrossRef\]](#)
47. Wang, Y.; Wang, J.; Yang, L.; Ma, B.; Sun, G.; Youssefi, N. Optimal designing of a hybrid renewable energy system connected to an unreliable grid based on enhanced African vulture optimizer. *ISA Trans.* **2022**. [\[CrossRef\]](#)
48. Fan, J.; Li, Y.; Wang, T. An improved African vultures optimization algorithm based on tent chaotic mapping and time-varying mechanism. *PLoS ONE* **2021**, *16*, e0260725. [\[CrossRef\]](#)
49. Mirza, A.F.; Mansoor, M.; Ling, Q.; Yin, B.; Javed, M.Y. A Salp-Swarm Optimization based MPPT technique for harvesting maximum energy from PV systems under partial shading conditions. *Energy Convers. Manag.* **2020**, *209*, 112625. [\[CrossRef\]](#)
50. Roy, R.B.; Rokonzaman, M.; Amin, N.; Mishu, M.K.; Alahakoon, S.; Rahman, S.; Pasupuleti, J. A comparative performance analysis of ANN algorithms for MPPT energy harvesting in solar PV system. *IEEE Access* **2021**, *9*, 102137–102152. [\[CrossRef\]](#)
51. National Renewable Energy Laboratory (NREL). Wind Prospector. 2022. Available online: <https://maps.nrel.gov/wind-prospector/?aL=0&bL=groad&cE=0&lR=0&mC=40.21244%2C-91.625976&zL=4%3Fvisible> (accessed on 20 May 2022).
52. Rao, C.S.; Santosh, S. Tuning optimal PID controllers for open loop unstable first order plus time delay systems by minimizing ITAE criterion. *IFAC Pap.* **2020**, *53*, 123–128. [\[CrossRef\]](#)
53. Bataineh, K. Improved hybrid algorithms-based MPPT algorithm for PV system operating under severe weather conditions. *IET Power Electron.* **2019**, *12*, 703–711. [\[CrossRef\]](#)
54. Duman, S.; Yorukeren, N.; Altas, I.H. A novel MPPT algorithm based on optimized artificial neural network by using FPSOGSA for standalone photovoltaic energy systems. *Neural Comput. Appl.* **2018**, *29*, 257–278. [\[CrossRef\]](#)
55. Abdollahzadeh, B.; Gharehchopogh, F.S.; Mirjalili, S. African vultures optimization algorithm: A new nature-inspired metaheuristic algorithm for global optimization problems. *Comput. Ind. Eng.* **2021**, *158*, 107408. [\[CrossRef\]](#)
56. MathWorks Inc. MATLAB 2016b. 2016. Available online: <https://www.mathworks.com/> (accessed on 1 June 2016).